D1.2
Analytical scattering theory

General information	
Grant agreement number	755500
Start date of the project	01/09/2017
Project duration	48 months
Due date of the deliverable	28/02/2019
Actual submission date	29/10/2020
Lead beneficiary	3 – FRAUNHOFER

Keywords
Scattering, perturbation theory, transversely isotropic material, attenuation, wave propagation

Type	Meaning	
R	Document, report	
DEM	Demonstrator, pilot, prototype	
DEC	Websites, patent fillings, videos, etc.	
OTHER	Software, technical diagram, etc.	x

Dissemination Level		
PU	Public	x
CO	Confidential, only for members of the consortium (including the Commission Services)	

Table of Contents

Table of Tables

Table of Figures

Glossary

Abbreviations/Acronym	Description
GPSS	General Purpose Simulation System
GUI	Graphical User Interface
qP wave	quasi-compressional wave
qSV wave	vertical polarized quasi-shear wave
SH wave	shear-horizontal wave

1 Executive Summary

This report discusses the basic concepts and results of Fraunhofer's semi-analytical scattering model.

Starting from the fundamental equation of motion for wave propagation in elastic media, perturbations to a presumed „ground state" elastic tensor allow for the calculation of scattering-induced attenuation. This perturbation theory is solved with second order. Utilizing an appropriate statistical scheme over elementary material configurations, effective propagation and attenuation parameters (complex k-vectors) for the three different wave modes (qP, qSV, SH) in transversely isotropic materials are derived, from which more handy effective elastic stiffness tensor elements follow. Hence, this work supports the understanding of how attenuation is related to scattering and how complex material properties can evolve from simpler setups as well. The corresponding implementation serves as a demonstrator for the interoperability of different partner tools (here esp. CIVA).

2 Introduction

Given the industrial application targeted by the project, the models used in the inspection technique design and data analysis tasks must be reasonably fast. To that end, fast semi-analytical models requiring wave-type specific scattering characteristics are developed, picking up progress made in the SIMPOSIUM FP7 project[1], which delivered these scattering characteristics for quasi-isotropic material configurations. For the needs within the ADVISE project, this approach must be pursued up to scattering models in inhomogeneous, anisotropic materials. Accordingly, the theoretical background to account for scattering effects in polycrystalline media is developed for textured grain orientations. The objective is to derive expressions for the wavetype-specific scattering coefficients for transverse and longitudinal waves in the quasi-isotropic case and for the quasi-longitudinal and the two quasi-transverse waves in the case of textured media. In view of an effective media approach, complex frequency-dependent wave vectors are extracted for an ultimate use within the CIVA platform. Furthermore, the derived complex frequency-dependent wave vectors should be used for an integration into the semi-analytical simulation approach, based on a geometric model to realistically simulate the microstructure.

---

[1] https://cordis.europa.eu/project/id/285549

3 Scattering Theory

The following describes the theory needed to derive the frequency-dependent complex wave vectors for textured polycrystalline media. With the imaginary part of such a wave vector, attenuation due to ultrasonic scattering is described. The derived complex wave vectors could be used for an integration into semi-analytical simulation approaches, such as the 'Generalized Point Source Superposition' (GPSS) developed at Fraunhofer. Furthermore, an attempt was made to pick up progress made in the SIMPOSIUM FP7 project. The SIMPOSIUM approach uses the scattering wave energy flux densities in microscopically inhomogeneous materials, which are formally derived from the infinite Born series presentation of ultrasonic displacement vectors. As a result one obtains directional and frequency-dependent scattering wave amplitudes for quasi-isotropic material configurations. Using the same approach, an attempt was made to find a solution for textured media.

The solutions of the elastodynamic equation of motion use a Green's function. Since no valid Green's function in position space can be found for the textured case (only a momentum space representation is available), this approach cannot be solved completely here. For this reason, frequency-dependent scattering wave amplitudes cannot be given for direct integration into CIVA, and another way had to be found. By calculating complex stiffness matrices, the derived complex wave vectors for textured media can be integrated into CIVA.

First, the derivation of the theory for the case of a transversely isotropic texture describing the structure of the austenitic weld is performed. Therefore, it is convenient to assume that all columnar crystals are aligned exactly vertically. Since this orientation will not be given in practice, another case should be considered in the theoretical derivation. Therefore, the horizontal case was considered in the second section. However, in general any orientation can be generated by coordinate transformation (as described in chapter 3.1.2).

3.1 Determination of complex wavenumbers for solids with transversely isotropic texture

Analogous to [1] the complex propagation constants of plane ultrasonic waves are now calculated from the solutions of the equation of motion of the displacement vector, which are approximately determined with the application of perturbation theory (equivalent to the Born approximation). Perturbation theory is solved with second order. The second order approximation was chosen because it yields the contribution of lowest order in the microscopic inhomogeneity if single-phase polycrystalline materials, in which the linear part of the ensemble average is zero, are considered. [2]

The model is derived for the case of cubic crystal symmetry and transversely isotropic texture (resp. hexagonal structure of the elasticity matrix). The microscopic cubic crystallites are described with a preferential orientation so that a macroscopic transversely isotropic texture results. As a result of the theoretical model one obtains direction-dependent complex propagation constants for different wave modes. For longitudinal waves the propagation constants can be described by

$$\beta_{LM} = k_p^M - i\alpha_{SL}^M,$$

where $M = 1,2,3$ denotes the vector index of propagation direction according to Figure 1, with k as wavenumber and α_s as scattering coefficient describing the attenuation due to ultrasonic scattering. In the case of a shear wave propagation the constant becomes

$$\beta_{TMP} = \kappa_p^{MP} - i\alpha_{ST}^{MP},$$

where $M, P = 1,2,3$ denotes the vector index of propagation respectively polarization direction. The wavenumber for shear waves is denoted by κ. The phase velocities (denoted by index p) v_{Lp}^M and v_{Tp}^{MP} are given by the wavenumbers

$$v_{Lp}^M = \frac{\omega}{k_p^M}$$

and

$$v_{Tp}^{MP} = \frac{\omega}{\kappa_p^{MP}}.$$

The representation as a function of angles of the propagation direction $\boldsymbol{e}_M$ is given by the wave vector

$$k^M = k_M \boldsymbol{e}_M,$$

$$\boldsymbol{e}_M = (n_{1M}, n_{2M}, n_{3M}) = (\sin\theta\cos\phi, \sin\theta\sin\phi, \cos\theta),$$

in case of compressional wave propagation and for the shear wave

$$\kappa^{MP} = \kappa_{MP} \boldsymbol{e}_M$$

$$\boldsymbol{e}_M = (n_{1M}, n_{2M}, n_{3M}), \quad \boldsymbol{e}_P = (n_{1P}, n_{2P}, n_{3P}),$$

according to the system of coordinates displayed in Figure 1. Note, that the characterization as longitudinal and shear accounts for the unperturbed (i.e. isotropic) system; $\boldsymbol{e}_M$ and $\boldsymbol{e}_P$ are not proper eigenvectors of the Christoffel matrix to be derived in the following, but represent the base for a typical perturbation ansatz.

If a mode-independent description is chosen, the theory describes in general a complex wavenumber

$$\tilde{k} = k - i\alpha_s,$$

using the real wavenumber and the ultrasonic attenuation described by the scattering coefficient α_s in the imaginary part.
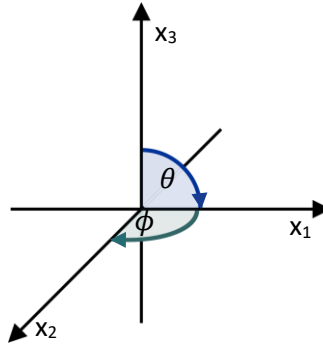
Figure 1 : system of coordinates

3.1.1 Vertically oriented transversely isotropic structure

The equation of motion of the complete displacement vector $\boldsymbol{s}$ in an inhomogeneous medium

$$\sum_{j,k,l=1}^{3} \frac{\partial}{\partial x_j}\left(C_{ijkl}\frac{\partial s_k}{\partial x_l}\right) + \rho\omega^2 s_i = 0$$

contains the incident wave $\boldsymbol{s}^0$ and all scattered waves $\boldsymbol{s}'$

$$\boldsymbol{s} = \boldsymbol{s}^0 + \boldsymbol{s}'.$$

The elastic constants C_{ijkl} and the density are in general position dependent in an inhomogenous medium.

The zeroth order of the equation of motion is chosen to be homogeneous and isotropic, with wavenumbers k for longitudinal waves and κ for shear waves. Let $\rho_0 = <\rho>$ be the mean of the density ρ and $<C_{ijkl}>$ the mean of the elastic constants C_{ijkl}, using ρ' and C'_{ijkl} as deviations one can use

$$\rho = \rho_0 + \rho' \quad \text{and} \quad C_{ijkl} = <C_{ijkl}> + C'_{ijkl}.$$

In case of cubic crystal symmetry and orthorhombic texture, the perturbational expansion of the equation of motion results in an infinite system of equations

$$\frac{\rho_0\omega^2}{k^2}\sum_{j=1}^{3}\frac{\partial^2 s_j^0}{\partial x_i \partial x_j} + \frac{\rho_0\omega^2}{\kappa^2}\frac{\partial}{\partial x_j}\left(\frac{\partial s_i^0}{\partial x_j}-\frac{\partial s_j^0}{\partial x_i}\right) + \rho_0\,\omega^2 s_i^0 = 0, \tag{1}$$

$$\frac{\rho_0\omega^2}{k^2}\sum_{j=1}^{3}\frac{\partial^2 s_j^{1\prime}}{\partial x_i \partial x_j} + \frac{\rho_0\omega^2}{\kappa^2}\frac{\partial}{\partial x_j}\left(\frac{\partial s_i^{1\prime}}{\partial x_j}-\frac{\partial s_j^{1\prime}}{\partial x_i}\right) + \rho_0\omega^2 s_i^{1\prime} = \frac{\rho_0\omega^2}{k^2}\,B_i^0 - \sum_{j=1}^{3}l_{ij}\frac{\partial^2 s_j^0}{\partial x_i \partial x_j} - \sum_{j=1}^{3}t_{ij}\frac{\partial}{\partial x_j}\left(\frac{\partial s_i^0}{\partial x_j}-\frac{\partial s_j^0}{\partial x_i}\right), \tag{2}$$

$$\frac{\rho_0\omega^2}{k^2}\sum_{j=1}^{3}\frac{\partial^2 s_j^{\nu\prime}}{\partial x_i \partial x_j} + \frac{\rho_0\omega^2}{\kappa^2}\frac{\partial}{\partial x_j}\left(\frac{\partial s_i^{\nu\prime}}{\partial x_j}-\frac{\partial s_j^{\nu\prime}}{\partial x_i}\right) + \rho_0\omega^2 s_i^{\nu\prime}$$

$$= \frac{\rho_0\omega^2}{k^2}\,B_i^{(\nu-1)\prime} - \sum_{j=1}^{3}l_{ij}\frac{\partial^2 s_j^{(\nu-1)\prime}}{\partial x_i \partial x_j} - \sum_{j=1}^{3}t_{ij}\frac{\partial}{\partial x_j}\left(\frac{\partial s_i^{(\nu-1)\prime}}{\partial x_j}-\frac{\partial s_j^{(\nu-1)\prime}}{\partial x_i}\right), \qquad \nu > 1. \tag{3}$$
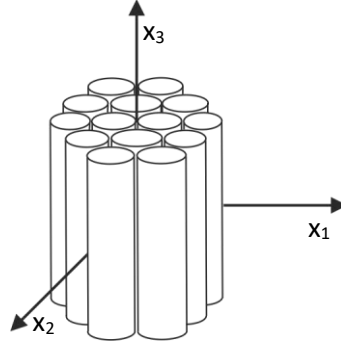

Figure 2 : vertical orientation of columnar crystals

The axes of the system of coordinates are chosen to be parallel to the symmetry directions of texture (see Figure 2). The function $\boldsymbol{B}^0$ and $\boldsymbol{B}^{\nu\prime}$ are given by

$$B_i^0 = -\left[\frac{\omega^2}{v_L^2}\frac{\rho'}{\rho_0}s_i^0 + \sum_{j,k,l=1}^{3}\frac{\partial}{\partial x_j}\left(\frac{C'_{ijkl}}{\rho_0 v_L^2}\frac{\partial s_k^0}{\partial x_l}\right)\right], \tag{4}$$

$$B_i^{\nu\prime} = -\left[\frac{\omega^2}{v_L^2}\frac{\rho'}{\rho_0}s_i^{\nu\prime} + \sum_{j,k,l=1}^{3}\frac{\partial}{\partial x_j}\left(\frac{C'_{ijkl}}{\rho_0 v_L^2}\frac{\partial s_k^{\nu\prime}}{\partial x_l}\right)\right], \qquad \nu \geq 1. \tag{5}$$

It contains the deviations of the real material constants from its mean values. The constants l_{ij} and t_{ij} are defined by

$$l_{ij} = \begin{cases} <C_{iiii}> -\dfrac{\rho_0\omega^2}{k^2}, & i = j, \\[2ex] <C_{iijj}> +2<C_{ijij}> -\dfrac{\rho_0\omega^2}{k^2}, & i \neq j, \end{cases} \tag{6}$$

$$t_{ij} = \begin{cases} 0, & i = j, \\[2ex] <C_{ijij}> -\dfrac{\rho_0\omega^2}{\kappa^2}, & i \neq j. \end{cases} \tag{7}$$

It describes the deviation of the homogeneous anisotropic material characterized by the mean density ρ_0 and the averaged elastic constants $<C_{ijkl}>$ from the homogeneous isotropic approximation defined by the wavenumbers k and κ for longitudinal and shear waves, respectively.

The detailed determination of averaged elastic constants $<C_{ijkl}>$ is given in chapter 4.

A precondition for the validity of the system of equations (1)-(3) is the convergence of the defined infinite expansion of the displacement vector

$$\boldsymbol{s} = \boldsymbol{s}^0 + \boldsymbol{s}' = \boldsymbol{s}^0 + \boldsymbol{s}^{1\prime} + \boldsymbol{s}^{2\prime} + \cdots. \tag{8}$$

This is realized within a region of ka limited by the condition

$$ka \ll \frac{k}{\left(< (k_p - k)^2 >\right)^{\frac{1}{2}}},$$

where k_p is the wavenumber in the inhomogeneous polycrystalline medium and k the wavenumber in the used homogeneous approximation.

The complex propagation constants of the plane waves are determined by the averaged potentials $< \boldsymbol{\Delta} >$ and $< \boldsymbol{\Phi} >$ of the longitudinal parts $\boldsymbol{s}_1$ and the transverse parts $\boldsymbol{s}_2$ of the displacement vector

$$\boldsymbol{s} = \boldsymbol{s}_1 + \boldsymbol{s}_2.$$

The potentials $\boldsymbol{\Delta}$ and $\boldsymbol{\Phi}$ are given by

$$\nabla \cdot \boldsymbol{s} = \nabla \cdot \boldsymbol{s}_1 = \boldsymbol{\Delta} = \boldsymbol{\Delta}^0 + \boldsymbol{\Delta}' = \boldsymbol{\Delta}^0 + \boldsymbol{\Delta}^{1'} + \boldsymbol{\Delta}^{2'} + \cdots,$$
$$\nabla \times \boldsymbol{s} = \nabla \times \boldsymbol{s}_2 = \boldsymbol{\Phi} = \boldsymbol{\Phi}^0 + \boldsymbol{\Phi}' = \boldsymbol{\Phi}^0 + \boldsymbol{\Phi}^{1'} + \boldsymbol{\Phi}^{2'} + \cdots. \tag{9}$$

The infinite series given in (9) correspond to the perturbational expansion (8) of the displacement vector. The expansion coefficients of different order of potentials result from the system of equations (1)-(3) to

$$\boldsymbol{\Delta}^{1'}(\boldsymbol{r}) = -\frac{1}{4\pi} \int d^3r' \frac{e^{-ik|\boldsymbol{r}-\boldsymbol{r}'|}}{|\boldsymbol{r}-\boldsymbol{r}'|} \left[\nabla_{\boldsymbol{r}'} \cdot B^0(\boldsymbol{r}') - \frac{k^2}{\rho_0 \omega^2} \sum_{i,j=1}^{3} l_{ij} \frac{\partial^2}{\partial x_i'^2} \frac{\partial s_j^0(\boldsymbol{r}')}{\partial x_j'} \right],$$

$$\boldsymbol{\Delta}^{\nu'}(\boldsymbol{r}) = -\frac{1}{4\pi} \int d^3r' \frac{e^{-ik|\boldsymbol{r}-\boldsymbol{r}'|}}{|\boldsymbol{r}-\boldsymbol{r}'|} \left[\nabla_{\boldsymbol{r}'} \cdot B^{(\nu-1)'}(\boldsymbol{r}') - \frac{k^2}{\rho_0 \omega^2} \sum_{i,j=1}^{3} l_{ij} \frac{\partial^2}{\partial x_i'^2} \frac{\partial s_j^{(\nu-1)'}(\boldsymbol{r}')}{\partial x_j'} \right], \quad \nu > 1,$$

$$\boldsymbol{\Phi}^{1'}(\boldsymbol{r}) = -\frac{1}{4\pi} \frac{\kappa^2}{k^2} \int d^3r' \frac{e^{-i\kappa|\boldsymbol{r}-\boldsymbol{r}'|}}{|\boldsymbol{r}-\boldsymbol{r}'|} \left[\nabla_{\boldsymbol{r}'} \times B^0(\boldsymbol{r}') \right.$$
$$\left. -\frac{k^2}{\rho_0 \omega^2} \sum_{i,j=1}^{3} \nabla_{\boldsymbol{r}'} \times \left[(l_{ij} - t_{ij}) \frac{\partial}{\partial x_j'} \boldsymbol{e}_i + t_{ij} \frac{\partial}{\partial x_i'} \boldsymbol{e}_j \right] \frac{\partial s_j^0(\boldsymbol{r}')}{\partial x_i'} \right], \tag{10}$$

$$\boldsymbol{\Phi}^{\nu'}(\boldsymbol{r}) = -\frac{1}{4\pi} \frac{\kappa^2}{k^2} \int d^3r' \frac{e^{-i\kappa|\boldsymbol{r}-\boldsymbol{r}'|}}{|\boldsymbol{r}-\boldsymbol{r}'|} \left[\nabla_{\boldsymbol{r}'} \times B^{(\nu-1)'}(\boldsymbol{r}') \right.$$
$$\left. -\frac{k^2}{\rho_0 \omega^2} \sum_{i,j=1}^{3} \nabla_{\boldsymbol{r}'} \times \left[(l_{ij} - t_{ij}) \frac{\partial}{\partial x_j'} \boldsymbol{e}_i + t_{ij} \frac{\partial}{\partial x_i'} \boldsymbol{e}_j \right] \frac{\partial s_j^{(\nu-1)'}(\boldsymbol{r}')}{\partial x_i'} \right], \quad \nu > 1,$$

at positions $\boldsymbol{r}$ and $\boldsymbol{r}'$, respectively (cf. [3–5]). The term of zeroth order of the potentials results from

$$\boldsymbol{\Delta}^0 = \nabla \cdot \boldsymbol{s}^0, \quad \boldsymbol{\Phi}^0 = \nabla \times \boldsymbol{s}^0, \tag{11}$$

which are plane waves, on the basis of plane waves from the solution of the equation of motion in zeroth order.

In the following, the complex propagation constants are determined by prescribed incident ultrasonic waves in perturbation theory with second order, meaning expansion coefficients up to second order are considered.

3.1.1.1   Complex propagation constants of longitudinal waves with random propagation direction

In case of an incident longitudinal wave

$$\boldsymbol{s}^0(\boldsymbol{r},t) = \boldsymbol{s}^0(\boldsymbol{r})e^{i\omega t} = \boldsymbol{e}_M e^{-i(k^M \boldsymbol{r} - i\omega t)},$$
$$k^M = k_M \boldsymbol{e}_M,$$

which moves parallel to the direction defined by the unit vector

$$\boldsymbol{e}_M = (n_{1M}, n_{2M}, n_{3M}) = (\sin\theta\cos\phi, \sin\theta\sin\phi, \cos\theta),$$

it is convenient to choose $k = k^M$ and $\kappa = \kappa_I$. The magnitude of the wave vector k^M is given in Voigt notation by

$$\frac{\rho_0 \omega^2}{k_M^2} = <C_{MMMM}> = \sum_{i=1}^{3} <C_{iiii}> n_{iM}^4 + \sum_{\substack{i,j=1 \\ i \neq j}}^{3} (<C_{iijj}> + 2 <C_{ijij}>) n_{iM}^2 n_{jM}^2,$$

for orthorhombic-cubic material symmetry. κ_I is defined as wavenumber of shear waves in polycrystalline material without texture (isotropic case), this means in Voigt notation

$$\frac{\rho_0 \omega^2}{\kappa_I^2} = <C_{ijij}^I> = C_{44}^0 + \frac{1}{5}(C_{11}^0 - C_{12}^0 - 2C_{44}^0) = \rho_0 v_{TI}^2,$$

in case of cubic symmetry of single crystals with the elastic constants C_{11}^0, C_{12}^0 and C_{44}^0.

With the equations (10) and (11), the averaged potentials $<\Delta^0(r)> = \Delta^0(r)$, $<\Delta^{1'}(r)>$ and $<\Delta^{2'}(r)>$ defined by [4] could be determined. The averaged expansion coefficient of the first order reduces to zero. The result of the averaged potential for longitudinal waves in perturbation theory of second order $<\Delta'(r)> = <\Delta^{2'}(r)>$ is put into the known equation for the complex propagation constant

$$\beta_{LM} = k_M \left\{ 1 - \frac{1}{V_g} \int_{V_g} d^3r \frac{1}{\Delta^0(r)} \left(1 - \frac{i}{k_M} \nabla \cdot e_M \right) <\Delta'(r)> \right\},$$

where V_g denotes the volume of one grain.

In the following, single-phase polycrystals are considered, which means that deviations of density ρ' become zero. The solution has the form

$$\beta_{LM} = k_M \left[1 - \frac{1}{(4\pi)^3} \left(\frac{A}{\rho_0 v_{LM}^2} \right)^2 \left(-B_1^M + \frac{\kappa_I^2}{k_M^2} B_2^M \right) \right],$$

with $A = C_{11}^0 - C_{12}^0 - 2C_{44}^0$ as factor of anisotropy. Considering the symmetry conditions of the cubic-transversely isotropic material one obtains

$$B_1^M = 24\pi^3 \{ 2 \bar{M}_{1122} S_1^M + 4(\bar{M}_{1133} - \bar{M}_{1122}) S_2^M + (\bar{M}_{3333} - 6 \bar{M}_{1133} + 3 \bar{M}_{1122}) S_3^M \},$$

$$B_2^M = 96\pi^3 \{ -(\tilde{M}_{1133} + 2 \tilde{M}_{1122}) S_1^M + (3 \tilde{M}_{1133} - \tilde{M}_{3333}) S_2^M + (\tilde{M}_{3333} - 6 \tilde{M}_{1133} + 3 \tilde{M}_{1122}) S_3^M \},$$

with $\bar{M}$ and $\tilde{M}$ as infinite series of spherical Bessel and Hankel functions given in the appendix 9.2. In the implementation a series up to tenth order is used (first order for Rayleigh approximation). The quantities S_1^M, S_2^M and S_3^M are sums weighted with the components of the unit vector over mean values of products of rotational matrix elements given in [1]. For cubic single crystals with transversely isotropic texture all texture coefficients $C_l^{\mu\nu}$ with $\nu \neq 0$ become zero, except the coefficients C_4^{10}, C_6^{10} and C_8^{10} (see chapter 4).

3.1.1.2   Complex propagation constants of shear waves with random propagation and polarization direction

The determination of the complex propagation constants for plane transverse waves is similar to the derivation for longitudinal waves. Considered is an incident wave

$$s^0(r,t) = s^0(r)e^{i\omega t} = e_P e^{-i(\kappa^{MP} r - i\omega t)},$$

$$\kappa^{MP} = \kappa_{MP} e_M,$$

with unit vectors e_M and e_P in propagation and polarization direction, respectively. It is convenient to choose $k = k_I$ and $\kappa = \kappa_{MP}$. The polarization e_P depends on the considered mode. For an horizontal polarized shear wave (SH), the polarization is described by

$$e_P = \sin \phi \, e_1 - \cos \phi \, e_2$$

and for a vertical polarized quasi-shear wave

$$e_P = \cos\theta\cos\phi\, e_1 + \cos\theta\sin\phi\, e_2 - \sin\theta\, e_3\,.$$

The magnitude of the wave vector κ^{MP} is given in Voigt notation by

$$\frac{\rho_0\omega^2}{\kappa_{MP}^2} = <C_{MPMP}>$$

$$= \sum_{i=1}^{3} <C_{iiii}> n_{iM}^2 n_{iP}^2 + \sum_{\substack{i,j=1\\i\neq j}}^{3} \{(<C_{iijj}> + <C_{ijij}>)n_{iM}n_{iP}n_{jM}n_{jP} + <C_{ijij}> n_{iM}^2 n_{jP}^2\},$$

for orthorhombic-cubic material symmetry. Analogous to κ_I in case of incident longitudinal waves, here k_I is defined as wavenumber of longitudinal waves in polycrystalline material without texture (isotropic case), this means in Voigt notation

$$\frac{\rho_0\omega^2}{k_I^2} = <C_{iiii}^I> = C_{11}^0 + \frac{2}{5}(C_{11}^0 - C_{12}^0 - 2C_{44}^0) = \rho_0 v_{LI}^2.$$

With the equations (10) and (11), the averaged potentials $<\Phi^0(r)> = \phi^0(r)$, $<\Phi^{1\prime}(r)>$ and $<\Phi^{2\prime}(r)>$ could be determined. The averaged expansion coefficient of the first order reduces to zero. The result of the averaged potential for shear waves in perturbation theory of second order $<\Phi'(r)> = <\Phi^{2\prime}(r)>$ is put into the known equation for the complex propagation constant

$$\beta_{TMP} = \kappa_{MP}\left\{1 - \frac{1}{V_g}\int_{V_g} d^3r\, \frac{1}{\Phi_{MP}^0(r)}\left(1 - \frac{i}{\kappa_{MP}}\nabla\cdot e_{MP}\right)<\Phi_{MP}'(r)>\right\},$$

$$\Phi_{MP}^0 = \Phi^0\cdot e_{MP}, \qquad \Phi_{MP}' = \Phi'\cdot e_{MP}, \qquad e_{MP} = e_M\times e_P.$$

The solution of integrals has the form

$$\beta_{TMP} = \kappa_{MP}\left[1 - \frac{1}{(4\pi)^3}\left(\frac{A}{\rho_0 v_{TMP}^2}\right)\left(-D_1^{MP} + \frac{k_I^2}{\kappa_{MP}^2}D_2^{MP}\right)\right].$$

Considering the symmetry conditions of the cubic-transverse-isotropic material one obtains

$$D_1^{MP} = 24\pi^3\{(\bar{M}_{1133} + 2\bar{M}_{1122})S_4^{MP} + (\bar{M}_{3333} - 3\bar{M}_{1133})S_5^{MP} + (\bar{M}_{3333} - 6\bar{M}_{1133} + 3\bar{M}_{1122})S_6^{MP}\},$$

$$D_2^{MP} = -96\pi^3\{2\tilde{M}_{1122}S_4^{MP} + 4(\tilde{M}_{1133} - \tilde{M}_{1122})S_5^{MP} + (\tilde{M}_{3333} - 6\tilde{M}_{1133} + 3\tilde{M}_{1122})S_6^{MP}\},$$

with $\bar{M}$ and $\tilde{M}$ as infinite series of spherical Bessel and Hankel functions given in the appendix 9.2. In the implementation a series up to tenth order is used (first order for Rayleigh approximation). The quantities S_4^{MP}, S_5^{MP} and S_6^{MP} are sums weighted with the components of the unit vector over mean values of products of rotational matrix elements given in [1]. For cubic single crystals with transversely isotropic texture all texture coefficients $C_l^{\mu\nu}$ with $\nu\neq 0$ become zero, only the coefficients C_4^{10}, C_6^{10} and C_8^{10} are not equal to zero (see chapter 4).

3.1.2   Horizontally oriented transversely isotropic structure

First we attempted - analogous to the vertical case - to derive the different propagation constants. However, the explicit theoretical derivation is too time-consuming. The same result can also be achieved more easily by transformation into a second coordinate system, which is rotated accordingly. Therefore a coordinate transformation of the results for the vertical case was carried out for the horizontal case. We define a rotational matrix to rotate around the y-axis

$$R_y(\alpha) = \begin{pmatrix} \cos\alpha & 0 & \sin\alpha \\ 0 & 1 & 0 \\ -\sin\alpha & 0 & \cos\alpha \end{pmatrix}$$

and one to rotate around z-axis

$$R_z(\alpha) = \begin{pmatrix} \cos\alpha & -\sin\alpha & 0 \\ \sin\alpha & \cos\alpha & 0 \\ 0 & 0 & 1 \end{pmatrix}.$$

The coordinate transformation shown in Figure 3 can be achieved by

$$\begin{pmatrix} \bar{X} \\ \bar{Y} \\ \bar{Z} \end{pmatrix} = R_y(-270°)R_z(-270°) \begin{pmatrix} x \\ y \\ z \end{pmatrix}.$$
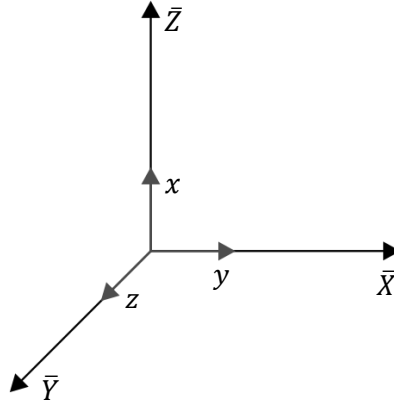

Figure 3 : coordinate transformation

To achieve a horizontal alignment of the columnar crystals in the coordinate system (see Figure 4), a rotation of 90° is used.
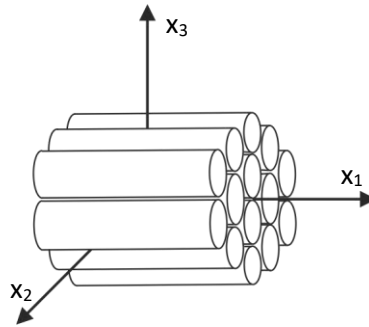
Figure 4 : horizontal orientation of columnar crystals

3.2   Assumptions in scattering theory and scope of application

To be able to compare the values calculated from the theory with measured values, the boundary conditions and restrictions of the model must be known. Thus, simplifications made in the model can be taken into account in the comparison, so that measurements are performed under similar conditions. For this reason all assumptions in the scattering model are listed below.

1) All grains have the same size and shape. Integrals over a grain volume are approximately equal to the corresponding integrals over a sphere of the same volume.
2) The probability of having a certain set of material constants is the same for all grains and is not affected by the adjacent grains.
3) The axes of the system of coordinates are chosen to be parallel to the symmetry directions of texture.
4) Since the equation of motion is solved by perturbation theory (equivalent to the Born approximation), one has to use a weak anisotropy condition, which leads to a limit of validity for large ka (k = wavenumber, a = grain radius). For a weakly anisotropic polycrystal the relative mean quadratic difference of the wavenumber k_p and k has to be much smaller than 1

$$\frac{<\left(k_p - k\right)^2>}{k^2} \ll 1,$$

where k_p is the wavenumber in the inhomogeneous polycrystalline medium and k the wavenumber in the used homogeneous approximation. This leads to a limit of theory by the relationship

$$ka \ll \frac{k}{\left(< \left(k_p - k \right)^2 > \right)^{\frac{1}{2}}} \; .$$

For a material with the parameters

$$v_{LI} = 5700 \, \frac{m}{s}$$
$$v_{TI} = 3140 \, \frac{m}{s}$$
$$C_{11}^0 = 2.16 \cdot 10^{11} \, Pa$$
$$C_{12}^0 = 1.45 \cdot 10^{11} \, Pa$$
$$C_{44}^0 = 1.29 \cdot 10^{11} \, Pa$$

the validity limits results in

$k_I a \ll 15.9$, for a longitudinal wave traveling in x_1-direction (perpendicular to the columnar crystals)

$k_I a \ll \infty$, for a longitudinal wave traveling in x_3-direction (in the direction of the columnar crystals)

$\kappa_I a \ll 4.98$, for a shear wave traveling in x_1-direction and polarization in x_2-direction (SH-wave travelling perpendicular to the direction of columnar crystals)

$\kappa_I a \ll \infty$, for a shear wave traveling in x_1-direction and polarization in x_3-direction (SV-wave travelling perpendicular to the direction of columnar crystals),

with $k_I = \frac{2\pi f}{v_{LI}}$ and $\kappa_I = \frac{2\pi f}{v_{TI}}$.

Thus the calculation is valid for waves with propagation or (and) polarization parallel to the axis of columnar crystals in the entire frequency range. For other wave modes, the validity range is still sufficient for a comparison with measured values.

An example of the validity limit is discussed in the following section.

3.3   Logarithmic Scaling for comparisons with measured values

The implementation of α_s from section 3.1.1 gives the attenuation due to scattering in the form of a factor with the unit $\frac{1}{m}$, which is rescaled to $\frac{1}{mm}$ for a realistic scale. If a logarithm is calculated to rescale the unit in $\frac{Np}{m}$ or $\frac{dB}{m}$ for a better comparability to measured values, the problem occurs that the influence of different unit scaling ($\frac{1}{m}$ or $\frac{1}{mm}$) is not linear in the logarithmic scaling. For this reason, the units have been normalized by division with the wavenumber, before the logarithmic scaling was used. The relation

$$-20 \cdot \log\left(\frac{\alpha_s}{k_I}\right) \cdot k_I \tag{12}$$

gives a unit in $\frac{dB}{m}$. Using (12) or its magnitude, all values are negative or do not have the same trend as without the logarithmic scaling. Therefore this scaling makes no sense and was brought to the same characteristic by using the inverse value. In addition, a factor of ten was used to compensate for the resulting too small scaling. In total, the following term was used for scaling in $\frac{dB}{m}$:

$$10 \cdot \left(-20 \cdot \log\left(\frac{\alpha_s}{k_I}\right) \right)^{-1} \cdot k_I \; .$$

The results are thus well comparable with the measured results from [6] (see Figure 5 - Figure 7).
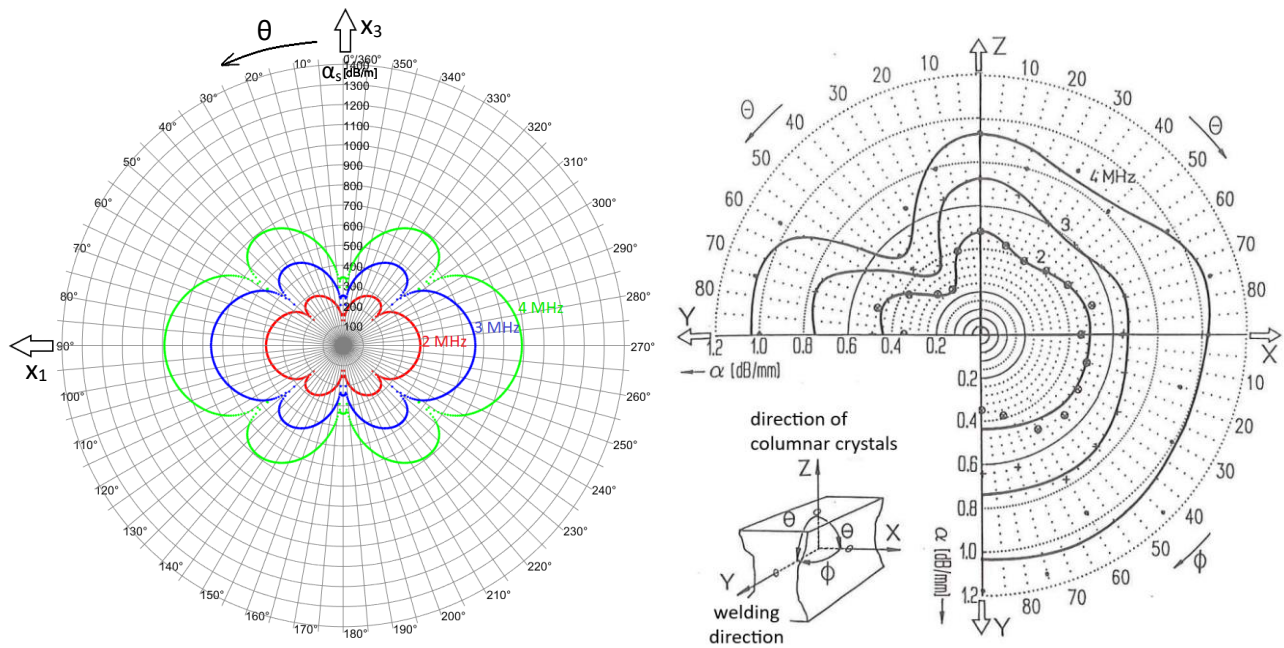
Figure 5 : directional dependent ultrasonic attenuation of quasi-longitudinal waves in austenitic weld X6 CrNi 18 11, left: calculated values, right: measured values from [6]
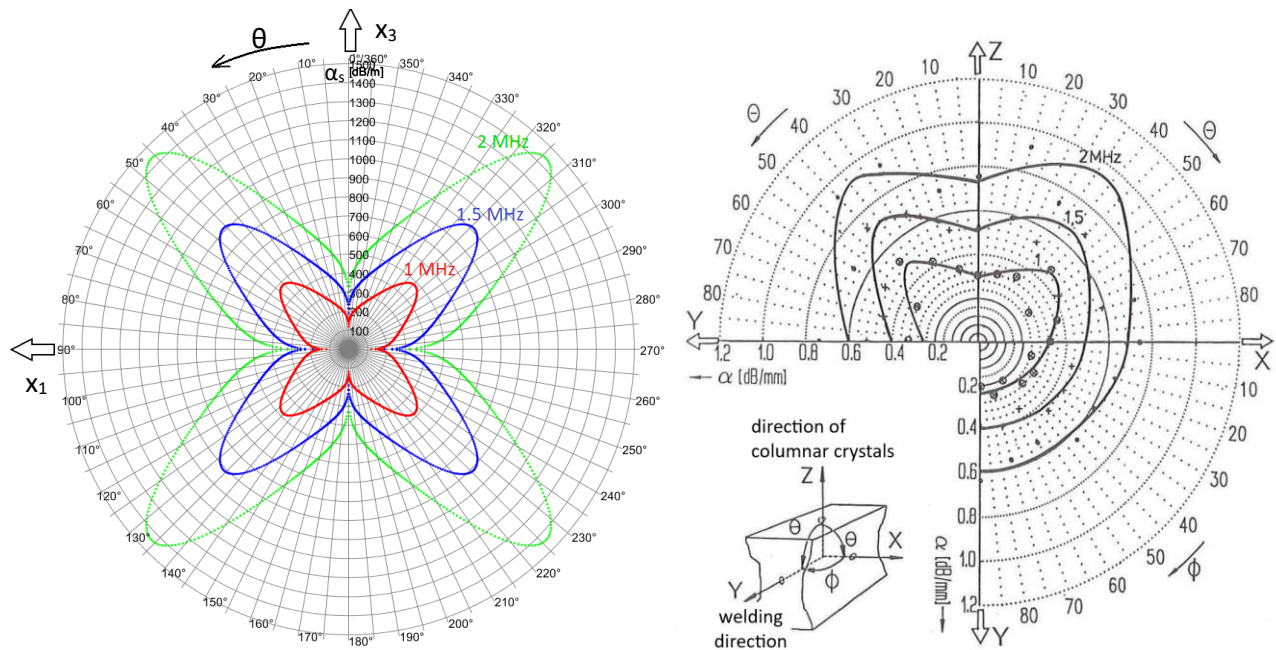

Figure 6 : directional dependent ultrasonic attenuation of vertical polarized quasi-shear waves in austenitic weld X6 CrNi 18 11, left: calculated values, right: measured values from [6]
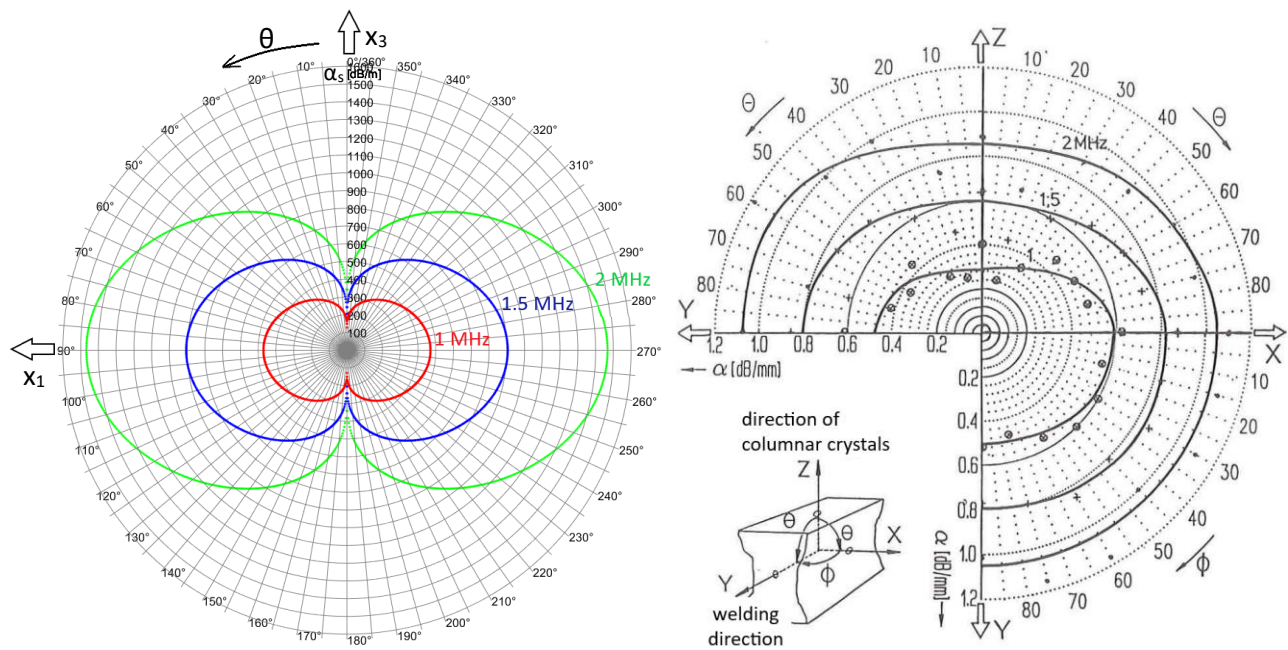
Figure 7 : directional dependent ultrasonic attenuation of horizontal polarized shear waves in austenitic weld X6 CrNi 18 11, left: calculated values, right: measured values from [6]

The values used for calculation are listed in Table 1.

material parameter	value	unit
isotropic longitudinal wave velocity	5700	m/s
isotropic shear wave velocity	3140	m/s
Density	7900	kg/m^3
C_{11}^0	$2.16 \cdot 10^{11}$	N/m^2
C_{12}^0	$1.45 \cdot 10^{11}$	N/m^2
C_{44}^0	$1.29 \cdot 10^{11}$	N/m^2
grain diameter	500	µm

Table 1: material parameter for X6 CrNi 18 11

In general, when comparing theory and measurement, the aperture angle of the ultrasonic beam must be taken into account. Since an ultrasonic beam always comprises more than just one angle, no direct agreement can be found with the theory for angle-dependent results. Therefore, an attempt was made to consider the angle of beam divergence by averaging the theoretical results. In Figure 8 - Figure 10 averaging was performed over an angular range of 20° (10° to the right and left each, around the mean value displayed). The 20° were chosen based on an estimation from [7]. Probably, an even larger angular range would need to be averaged for the shear waves. However, the aperture of the sound beam is strongly dependent on the probe used, the type of excitation and the distance. Due to the absence of information in the literature, from which the measured values are taken, this cannot be reproduced more precisely here. For a larger angle of beam spread, especially for the shear wave, the theory and measurement would match even better. Nevertheless, the consideration of the angular range of 20° already shows a better agreement between theory and measurement.
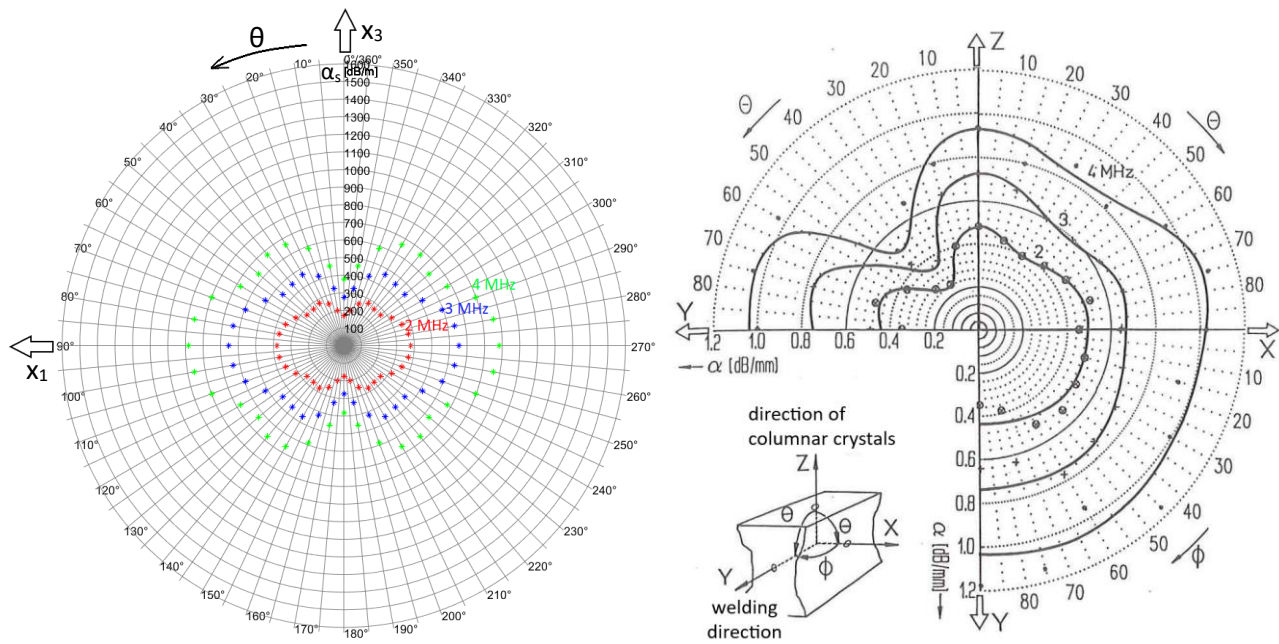
Figure 8 : directional dependent ultrasonic attenuation of quasi-longitudinal waves in austenitic weld X6 CrNi 18 11, left: averaged calculated values, right: measured values from [6]
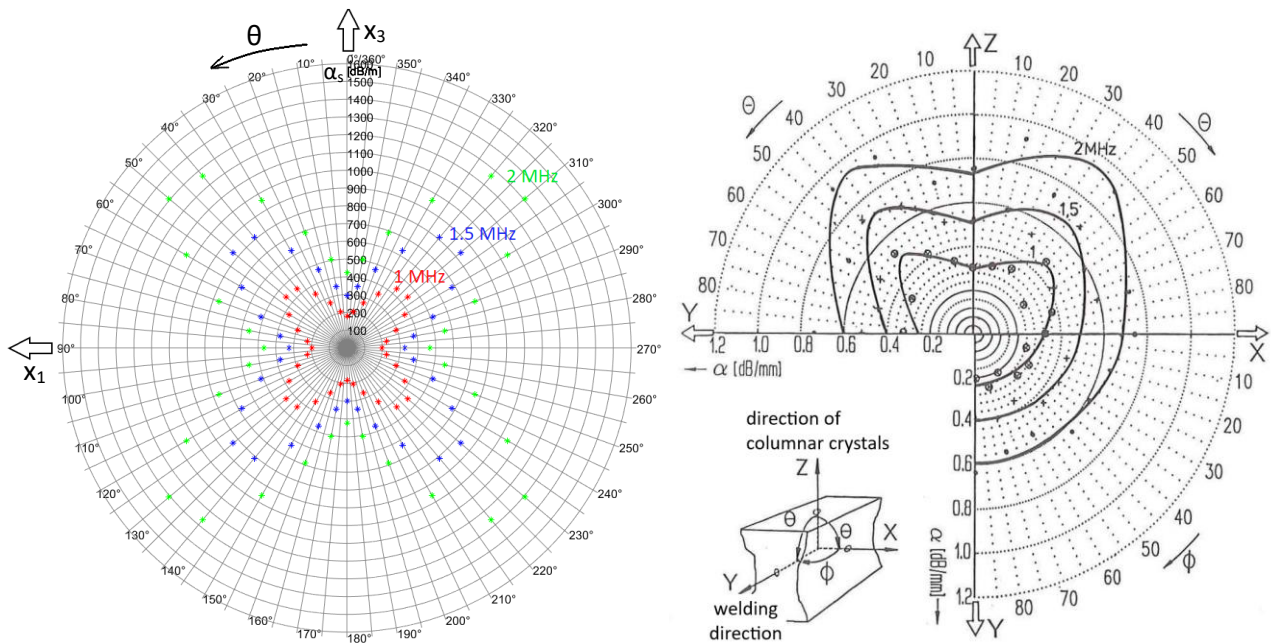
Figure 9 : directional dependent ultrasonic attenuation of vertical polarized quasi-shear waves in austenitic weld X6 CrNi 18 11, left: averaged calculated values, right: measured values from [6]
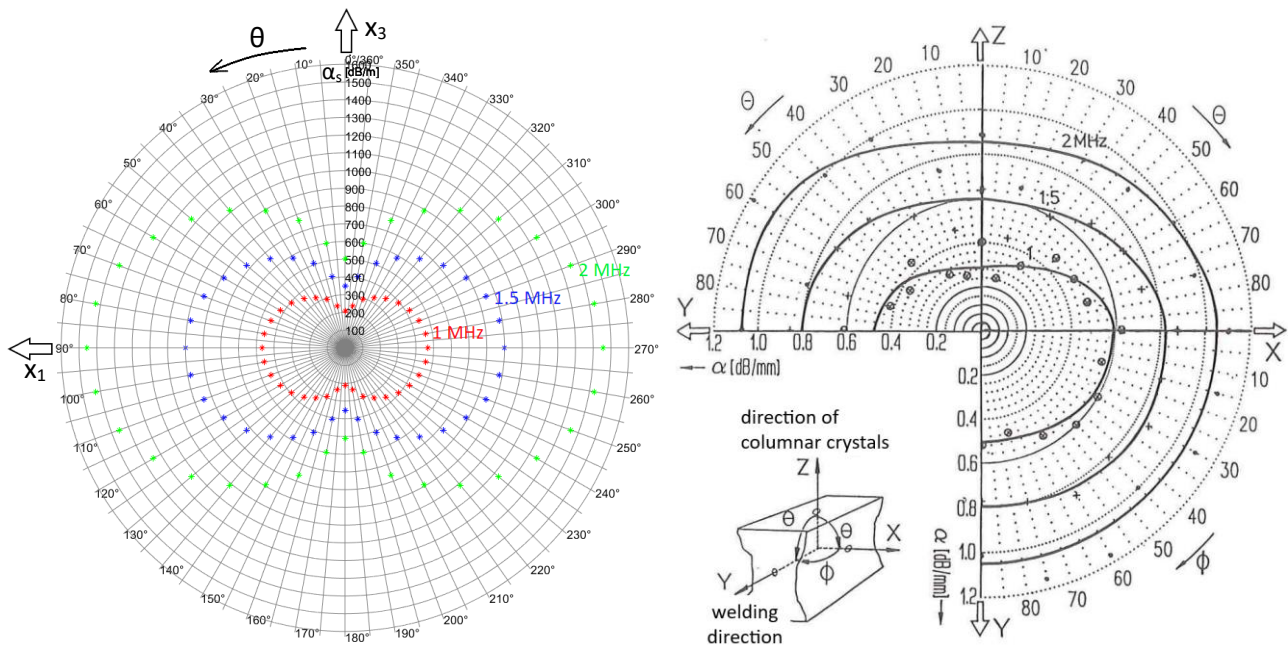
Figure 10 : directional dependent ultrasonic attenuation of horizontal polarized shear waves in austenitic weld X6 CrNi 18 11, left: averaged calculated values, right: measured values from [6]

In section 3.2 the scope of the theory was discussed. It can be stated that at least for some angles the validity limit is exceeded due to the very coarse grain structure. For grain diameters of 500 µm in this weld made of X6CrNi18 11 the limits of the longitudinal wave (in 90°) are 3 MHz and those of the SH waves (in 90°) are 0.5 MHz. For smaller grain sizes e.g. 100 µm the scope for longitudinal waves (in 90°) is 10 MHz and for SH waves (in 90°) it is 2.5 MHz, which are values that are more suitable.

The largest deviation between theory and measurement is obtained for all wave types in 0° and 90° direction. This is mainly explained by the approximations of the model. In a real weld, the columnar crystals are never aligned exactly parallel in the vertical direction and even small angular deviations have a significant influence on the result. Especially noticeable is the deviation of the longitudinal wave in 0° direction, although we suspect that numerical instabilities might also contribute.

4 Determination of real stiffness matrix according to Bunge

In the anisotropic case, the macroscopic texture is described by the orientation distribution function $f(\theta, \psi, \phi)$. This function indicates the probability to find a certain grain orientation. Therefore, the macroscopic constants C_{ij} are described by the elastic single crystal constants C_{ij}^0 and their rotation around the spherical angle $\Omega = (\theta, \psi, \phi)$. This context is illustrated in Figure 11, and in Voigt notation this yields:

$$C_{ij} = <C_{ijkl}> = \frac{1}{8\pi^2} \int_0^\pi \int_0^{2\pi} \int_0^{2\pi} \sin(\theta)\, d\theta d\psi d\phi\, f(\theta, \psi, \phi) C_{ijkl}^0(\theta, \psi, \phi)\,.$$

For representation of the orientation distribution function, the series expansions described by Bunge in [8] with generalized spherical functions T_l^{mn} are used.

$$f(\theta, \psi, \phi) = \sum_{l=0}^\infty \sum_{m,n=-l}^l c_l^{mn} T_l^{mn}(\theta, \psi, \phi)$$

The quantities c_l^{mn} are the expansion coefficients (not to be confused with the elastic constants C_{ijkl}). The symmetry of texture and single crystals reduces the number of linear independent expansion coefficients c_l^{mn}:

$$f(\theta, \psi, \phi) = \sum_{l=0}^\infty \sum_\mu \sum_\nu C_l^{\mu\nu} \dot{T}_l^{\mu\nu}(\theta, \psi, \phi)\,.$$

The functions $\dot{T}_l^{\mu\nu}$ are, with respect to symmetry of single crystal and texture, symmetrized generalized spherical functions. The number of linear independent expansion coefficients $C_l^{\mu\nu}$ (named **texture coefficients**) follows from symmetry of texture and single crystal and is dependent of the order l of expansion (here: l=8). In total, the elastic constants with macroscopic transversely isotropic texture and cubic single crystal symmetry are calculated by

$$<C_{ijkl}> = C_{12}^0 \delta_{ij}\delta_{kl} + C_{44}^0(\delta_{ik}\delta_{jl} + \delta_{il}\delta_{jk}) + (C_{11}^0 - C_{12}^0 - 2C_{44}^0) \sum_{\alpha=1}^3 <a_{\alpha i}a_{\alpha j}a_{\alpha k}a_{\alpha l}>, \qquad (13)$$

determining the mean value of a multiple product of rotation matrix elements $a_{\alpha i}$, with

$$(a_{\alpha i}) = \begin{pmatrix} \cos\psi\cos\phi - \cos\theta\cos\psi\sin\phi & \sin\psi\cos\phi + \cos\theta\cos\psi\sin\phi & \sin\theta\sin\phi \\ -\cos\psi\sin\phi - \cos\theta\sin\psi\cos\phi & -\sin\psi\sin\phi + \cos\theta\cos\psi\cos\phi & \sin\theta\cos\phi \\ \sin\theta\sin\psi & -\sin\theta\cos\psi & \cos\theta \end{pmatrix}$$

(cf. [9, 10]).

With an orientation of the columnar crystals in x₃ direction, f has the form

$$f(\theta, \psi, \phi) = C\Big\{[\delta(\cos\theta - 1) + \delta(\cos\theta + 1)]\delta(\phi)$$

$$+ \delta(\cos\theta)\Big[\delta(\phi) + \delta\left(\phi - \frac{\pi}{2}\right) + \delta(\phi - \pi) + \delta\left(\phi - \frac{3}{2}\pi\right)\Big]\Big\},$$

with $C = \frac{2}{3}\pi$ and δ as delta distribution.
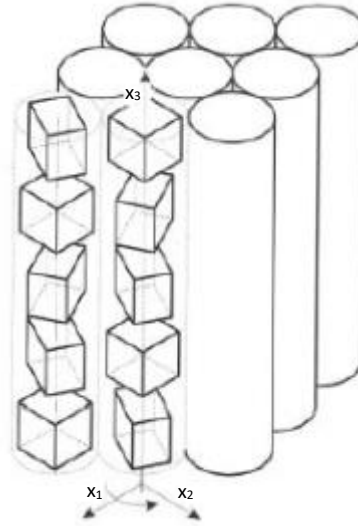
Figure 11 : statistical orientation of single crystals in x₁-x₂-plain, but preferential direction in x₃-direction leads to a macroscopic transversely isotropic (hexagonal) structure with columnar crystals (cf. [11])

The orientation distribution of cubic single crystals leads to a macroscopic transversely isotropic texture (hexagonal structure of stiffness matrix), with columnar crystals oriented in x_3-direction and an isotropic plane as x_1-x_2-plane (see Figure 12).
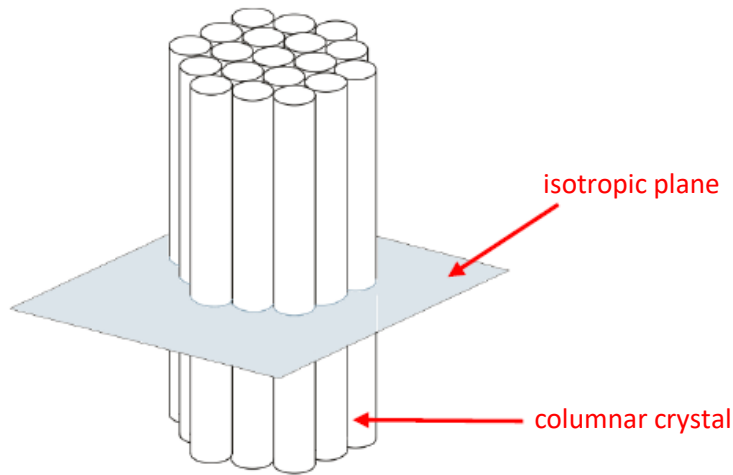
Figure 12 : columnar crystals with isotropic plane, described by the transversely isotropic texture (cf. [11])

Vertical orientation:

Calculating $< C_{ijkl} >$ after (13) with the calculated mean value of a multiple product of rotation matrix elements $a_{\alpha i}$ after [1, 3] (see appendix 9.1), we obtain the known transversely isotropic structure with five independent elastic constants of the following form:

$$C_{ij} = \begin{pmatrix} C_{11} & C_{12} & C_{13} & & & \\ C_{12} & C_{11} & C_{13} & & & \\ C_{13} & C_{13} & C_{33} & & & \\ & & & C_{55} & & \\ & & & & C_{55} & \\ & & & & & C_{66} \end{pmatrix}, \tag{14}$$

with $C_{66} = \frac{C_{11} - C_{12}}{2}$.

The macroscopic elastic constants results with texture coefficients $\boldsymbol{C_4^{10}} = \frac{3}{2}\sqrt{3 \cdot 7}$, $\boldsymbol{C_4^{11}} = 0$ and $\boldsymbol{C_4^{12}} = 0$ to:

$$C_{11} = C_{11}^0 - \frac{1}{4}A,$$

$$C_{33} = C_{11}^0,$$

$$C_{55} = C_{44}^0,$$

$$C_{66} = C_{44}^0 + \frac{1}{4}A,$$

$$C_{12} = C_{12}^0 + \frac{1}{4}A,$$

$$C_{13} = C_{12}^0,$$

with an anisotropy factor of $A = C_{11}^0 - C_{12}^0 - 2C_{44}^0$ (cf. [9]).

Horizontal orientation:

For an horizontal alignment of columnar crystals (see Figure 4) the calculation was done analogous to the vertical case. One obtains a transversely isotropic structure with five independent elastic constants of the following form

$$\bar{C}_{ij} = \begin{pmatrix} \bar{C}_{11} & \bar{C}_{12} & \bar{C}_{12} & & & \\ \bar{C}_{12} & \bar{C}_{22} & \bar{C}_{23} & & & \\ \bar{C}_{12} & \bar{C}_{23} & \bar{C}_{22} & & & \\ & & & \bar{C}_{44} & & \\ & & & & \bar{C}_{66} & \\ & & & & & \bar{C}_{66} \end{pmatrix}, \tag{15}$$

with $\bar{C}_{44} = \frac{\bar{C}_{22} - \bar{C}_{23}}{2}$.

The macroscopic elastic constants results with texture coefficients $C_4^{10} = \frac{9}{16}\sqrt{3 \cdot 7}$, $C_4^{11} = -\frac{3}{8}\sqrt{3 \cdot 5 \cdot 7}$ and $C_4^{12} = \frac{21}{16}\sqrt{3 \cdot 5}$ (derivation see 9.1.2) to:

$$\bar{C}_{11} = C_{11}^0,$$

$$\bar{C}_{22} = C_{11}^0 - \frac{1}{4}A,$$

$$\bar{C}_{44} = C_{44}^0 + \frac{1}{4}A,$$

$$\bar{C}_{66} = C_{44}^0,$$

$$\bar{C}_{12} = C_{12}^0,$$

$$\bar{C}_{23} = C_{12}^0 + \frac{1}{4}A,$$

with an anisotropy factor of $A = C_{11}^0 - C_{12}^0 - 2C_{44}^0$ and the relation $\bar{C}_{44} = \frac{1}{2}(\bar{C}_{22} - \bar{C}_{23})$.

5   Determination of complex stiffness matrix

The complex wavenumbers derived in section 3.1 could be used directly for an implementation in the GPSS algorithm by IZFP. For a plug-in into CIVA other values are needed. For that reason in the following, a complex stiffness tensor for implementation in CIVA will be derived, comparable to [12].

Chassignole et al. use [13, 14] as reference for the definition of the complex stiffness tensor. [14] is valid for orthotropic materials and uses the stiffness tensor as a viscoelastic complex tensor with nine independent constants:

$$C_{ij}^* = \begin{bmatrix} C_{11}^* & C_{12}^* & C_{13}^* & 0 & 0 & 0 \\ & C_{22}^* & C_{23}^* & 0 & 0 & 0 \\ & & C_{33}^* & 0 & 0 & 0 \\ & & & C_{44}^* & 0 & 0 \\ & Sym & & & C_{55}^* & 0 \\ & & & & & C_{66}^* \end{bmatrix},$$

where $[C_{ij}^*] = [C_{ij}'] + i[C_{ij}'']$.

C_{ij}' are the elastic constants of the material and C_{ij}'' are its viscoelastic constants that represent the attenuating material properties.

Viscoelastic constants represent the attenuating material properties due to damping. The damping is caused by absorption. The oscillatory motion of particles in this medium is damped by internal friction, elastic hysteresis, heat generation, relaxational phenomena, etc.

In [13], a complex stiffness matrix is given as $C_{ij}^* = C_{ij} + J\omega\eta_{ij}$, where η_{ij} are the viscosity constants. The paper describes the losses in orthotropic composite materials, which have viscoelastic properties. A relation is defined between a complex wave vector k as

$$k_j^* = k_j - Jk_j'',$$

with k'' as damping vector and the viscosity constants η_{ij}. In addition, the losses in the composite material were measured with ultrasound.

In [12] tensors C and D are used, which describe the stiffness and attenuation following the equation

$$\frac{\partial \sigma}{\partial t} + D\sigma = C\varepsilon,$$

where ε, σ are strain and stress tensors. Equations without attenuation are found for D equal to zero, and C, therefore, refers to the material's elasticity tensor. In the model with attenuation, Christoffel tensors are constructed from complex tensor $\bar{C}$ following the approach by Hosten [13]:

$$\bar{C} = i\omega(i\omega + D)^{-1}C,$$

where ω is the angular frequency. In this case, the Christoffel eigenvalues are not anymore ρV_p^2 and ρV_T^2 but complex expressions:

$$\Lambda_P = \rho \left(\frac{V_P}{1 - i\frac{\gamma_p V_P}{\omega}} \right)^2$$

$$\Lambda_T = \rho \left(\frac{V_T}{1 - i\frac{\gamma_T V_T}{\omega}} \right)^2,$$

where γ_P and γ_T are attenuations, with longitudinal and transverse wave velocities v_L and v_T.

The attenuation calculated by Faunhofer IZFP is a scattering coefficient describing the attenuation due to ultrasonic scattering, typically leading to a different behaviour in the frequency domain when compared to viscous damping. Viscous damping is not considered here.

It is known that for example in steel and castings the attenuation due to ultrasonic scattering has a much stronger influence than attenuation due to damping. Taking this into account, the values for γ_P and γ_T could be represented by values calculated by IZFP as attenuation due to scattering. Nevertheless, the aim is the calculation of attenuation for anisotropic (hexagonal resp. transversely isotropic) structures. Therefore, the Christoffel eigenvalues should become angle dependent and the above relations cannot simply be used. Following [15] a complex stiffness tensor for the transversely isotropic case is derived.

A harmonic plane wave in an attenuative medium has a displacement

$$u = \hat{u} \exp(i(\omega t - \tilde{k}x)), \tag{16}$$

where $\hat{u}$ is the polarization vector, ω the angular frequency, t the time and $\tilde{k}$ the complex wave vector. The wave vector $\tilde{k}$ becomes complex in the presence of attenuation with the wavenumber k in the real part and the attenuative part in the imaginary part. In this case, we use only attenuation due to ultrasonic scattering so that the imaginary part of $\tilde{k}$ is described by the ultrasonic scattering coefficient:

$$\tilde{k} = k - i\alpha_s .$$

Substitution of equation (16) into the equation of motion

$$\tilde{C}_{ijkl} \frac{\partial^2 u_k}{\partial x_l \partial x_j} = \rho \ddot{u}_i, \quad i,j = 1,2,3 \tag{17}$$

yields the Christoffel equation

$$\left[\tilde{C}_{ijkl} n_j n_l - \rho \tilde{v}^2 \delta_{ik}\right] \hat{u}_k = 0 . \tag{18}$$

Where, $\tilde{C}_{ijkl} = C_{ijkl} + iC^I_{ijkl}$ is the complex stiffness, n is the phase direction, ρ is the density, δ_{ik} is Kronecker's delta and $\tilde{v}$ is the complex phase velocity as $\tilde{v} = \frac{\omega}{\tilde{k}} = \frac{v}{\left(1 - i\frac{\alpha_S}{k}\right)}$ with $v = \frac{\omega}{k}$.

Thus, with the Christoffel tensor

$$\bar{\Gamma}_{ik} = \sum_{j=1}^{3} \sum_{l=1}^{3} \tilde{C}_{ijkl} n_j n_l, \quad i,j = 1,2,3, \tag{19}$$

one obtains the following eigenvalue problem

$$\begin{bmatrix} \bar{\Gamma}_{11} - \rho \tilde{v}^2 & \bar{\Gamma}_{12} & \bar{\Gamma}_{13} \\ \bar{\Gamma}_{12} & \bar{\Gamma}_{22} - \rho \tilde{v}^2 & \bar{\Gamma}_{23} \\ \bar{\Gamma}_{13} & \bar{\Gamma}_{23} & \bar{\Gamma}_{33} - \rho \tilde{v}^2 \end{bmatrix} \begin{bmatrix} \hat{u}_1 \\ \hat{u}_2 \\ \hat{u}_3 \end{bmatrix} = \begin{bmatrix} 0 \\ 0 \\ 0 \end{bmatrix}, \tag{20}$$

which can be solved for different directions to derive the complex stiffness tensor.

Using the symmetry conditions, Equation (19) gives

$$\begin{aligned} \bar{\Gamma}_{11} &= \tilde{C}_{11} n_1^2 + \tilde{C}_{66} n_2^2 + \tilde{C}_{55} n_3^2 \\ &= C_{11} n_1^2 + C_{66} n_2^2 + C_{55} n_3^2 + i \left[C^I_{11} n_1^2 + C^I_{66} n_2^2 + C^I_{55} n_3^2 \right] \\ \bar{\Gamma}_{22} &= C_{66} n_1^2 + C_{22} n_2^2 + C_{44} n_3^2 + i \left[C^I_{66} n_1^2 + C^I_{22} n_2^2 + C^I_{44} n_3^2 \right] \\ \bar{\Gamma}_{33} &= C_{55} n_1^2 + C_{44} n_2^2 + C_{33} n_3^2 + i \left[C^I_{55} n_1^2 + C^I_{44} n_2^2 + C^I_{33} n_3^2 \right] \\ \bar{\Gamma}_{12} &= (C_{12} + C_{66}) n_1 n_2 + i \left[(C^I_{12} + C^I_{66}) n_1 n_2 \right] \\ \bar{\Gamma}_{13} &= (C_{13} + C_{55}) n_1 n_3 + i \left[(C^I_{13} + C^I_{55}) n_1 n_3 \right] \\ \bar{\Gamma}_{23} &= (C_{23} + C_{44}) n_2 n_3 + i \left[(C^I_{23} + C^I_{44}) n_2 n_3 \right] \end{aligned}$$

Depending on the considered direction, vertical or horizontal orientation of the columnar crystals, C_{ij} has to be replaced by $\bar{C}_{ij}$ and the following symmetry conditions apply:

$$C_{44} = C_{55}, C_{11} = C_{22}, C_{13} = C_{23}, \text{ resp. } \bar{C}_{55} = \bar{C}_{66}, \bar{C}_{22} = \bar{C}_{33}, \bar{C}_{12} = \bar{C}_{13}.$$

Assuming that a plane wave propagates in the x_1-x_3-plane in the direction of θ in relation to the x_3-axis (see Figure 1). With the assumed fiber direction in Figure 2, the values for n_j result to $n_1 = \sin\theta$, $n_2 = 0, n_3 = \cos\theta$. To find the eigenvalues of Eq. (20) one implement the zero-determinant condition.

Case 1

Set $\theta = 0°$ and thus $n = (0,0,1)^T$, it follows

$$\begin{vmatrix} C_{55} + iC_{55}^I - \rho\tilde{v}^2 & 0 & 0 \\ 0 & C_{44} + iC_{44}^I - \rho\tilde{v}^2 & 0 \\ 0 & 0 & C_{33} + iC_{33}^I - \rho\tilde{v}^2 \end{vmatrix} = 0. \tag{21}$$

Defining $A_s = \frac{\alpha_s}{k}$ and using

$$\tilde{v}^2 = \left(\frac{v}{\left(1 - i\frac{\alpha_s}{k}\right)}\right)^2 = \frac{v^2(1 - A_s^2)}{(1 + A_s^2)^2} + i\left(\frac{2v^2 A_s}{(1 + A_s^2)^2}\right)$$

one obtains, as roots

$$\Lambda_1 = C_{33} + i\, C_{33}^I - \rho\left(\frac{v^2(1 - A_s^2)}{(1 + A_s^2)^2} + i\left(\frac{2v^2 A_s}{(1 + A_s^2)^2}\right)\right),$$

$$\Lambda_2 = C_{44} + i\, C_{44}^I - \rho\left(\frac{v^2(1 - A_s^2)}{(1 + A_s^2)^2} + i\left(\frac{2v^2 A_s}{(1 + A_s^2)^2}\right)\right),$$

$$\Lambda_3 = C_{55} + i\, C_{55}^I - \rho\left(\frac{v^2(1 - A_s^2)}{(1 + A_s^2)^2} + i\left(\frac{2v^2 A_s}{(1 + A_s^2)^2}\right)\right),$$

with the corresponding eigenvectors $\xi_1 = (0,0,1)^T, \xi_2 = (0,1,0)^T, \xi_3 = (1,0,0)^T$.

As eigenvalues, one obtains the several ultrasonic velocities for the different particle displacements and thus the entries for the complex stiffness matrix. The first eigenvalue gives

$$C_{33} = \rho\left(\frac{v_L^2(0°)\left(1 - A_{s_L}^2(0°)\right)}{\left(1 + A_{s_L}^2(0°)\right)^2}\right)$$

and

$$C_{33}^I = \rho\left(\frac{2v_L^2(0°)A_{s_L}(0°)}{\left(1 + A_{s_L}^2(0°)\right)^2}\right),$$

because the corresponding eigenvector ξ_1 provide the particle displacements occurring in propagation direction and thus describing a quasi-longitudinal wave. The second eigenvalue gives

$$C_{44} = \rho\left(\frac{v_{SH}^2(0°)\left(1 - A_{s_{SH}}^2(0°)\right)}{\left(1 + A_{s_{SH}}^2(0°)\right)^2}\right)$$

and

$$C_{44}^I = \rho\left(\frac{2v_{SH}^2(0°)A_{s_{SH}}(0°)}{\left(1 + A_{s_{SH}}^2(0°)\right)^2}\right),$$

because the corresponding eigenvector ξ_2 provide the particle displacements occurring perpendicular to the propagation direction polarized in x_2-direction and thus describing a shear horizontal (SH) wave. The third eigenvalue gives

$$C_{55} = \rho \left(\frac{v_{SV}^2(0°)\left(1 - A_{S_{SV}}^2(0°)\right)}{\left(1 + A_{S_{SV}}^2(0°)\right)^2} \right)$$

and

$$C_{55}^I = \rho \left(\frac{2v_{SV}^2(0°)A_{S_{SV}}(0°)}{\left(1 + A_{S_{SV}}^2(0°)\right)^2} \right),$$

because the corresponding eigenvector ξ_3 provide the particle displacements occurring perpendicular to the propagation direction polarized in x_1-direction and thus describing a vertical polarized quasi-shear (SV) wave.

Case 2

In this case set $\theta = 90°$ and thus $n = (1,0,0)^T$, so that

$$\begin{vmatrix} C_{11} + iC_{11}^I - \rho\tilde{v}^2 & 0 & 0 \\ 0 & C_{66} + iC_{66}^I - \rho\tilde{v}^2 & 0 \\ 0 & 0 & C_{55} + iC_{55}^I - \rho\tilde{v}^2 \end{vmatrix} = 0, \tag{22}$$

with roots

$$\Lambda_1 = C_{11} + i\,C_{11}^I - \rho\tilde{v}^2,$$
$$\Lambda_2 = C_{55} + i\,C_{55}^I - \rho\tilde{v}^2,$$
$$\Lambda_3 = C_{66} + i\,C_{66}^I - \rho\tilde{v}^2,$$

and the corresponding eigenvectors $\xi_1 = (1,0,0)^T, \xi_2 = (0,0,1)^T, \xi_3 = (0,1,0)^T$.

The first eigenvalue gives

$$C_{11} = \rho \left(\frac{v_L^2(90°)\left(1 - A_{S_L}^2(90°)\right)}{\left(1 + A_{S_L}^2(90°)\right)^2} \right)$$

and

$$C_{11}^I = \rho \left(\frac{2v_L^2(90°)A_{S_L}(90°)}{\left(1 + A_{S_L}^2(90°)\right)^2} \right),$$

the second

$$C_{55} = \rho \left(\frac{v_{SV}^2(90°)\left(1 - A_{S_{SV}}^2(90°)\right)}{\left(1 + A_{S_{SV}}^2(90°)\right)^2} \right)$$

and

$$C_{55}^I = \rho \left(\frac{2v_{SV}^2(90°)A_{S_{SV}}(90°)}{\left(1 + A_{S_{SV}}^2(90°)\right)^2} \right),$$

and the third

$$C_{66} = \rho \left(\frac{v_{SH}^2(90°)\left(1 - A_{S_{SH}}^2(90°)\right)}{\left(1 + A_{S_{SH}}^2(90°)\right)^2} \right)$$

and

$$C_{66}^I = \rho \left(\frac{2v_{SH}^2(90°)A_{S_{SH}}(90°)}{\left(1 + A_{S_{SH}}^2(90°)\right)^2} \right),$$

in the same manner as in the first case.

Case 3

Here, set $\theta = 45°$ and so that $n = \left(\frac{1}{\sqrt{2}}, 0, \frac{1}{\sqrt{2}}\right)^T$, it follows

$$
\begin{vmatrix}
\frac{1}{2}(\tilde{C}_{11} + \tilde{C}_{55}) - \rho\tilde{v}^2 & 0 & \frac{1}{2}(\tilde{C}_{13} + \tilde{C}_{55}) \\
0 & \frac{1}{2}(\tilde{C}_{66} + \tilde{C}_{44}) - \rho\tilde{v}^2 & 0 \\
\frac{1}{2}(\tilde{C}_{13} + \tilde{C}_{55}) & 0 & \frac{1}{2}(\tilde{C}_{33} + \tilde{C}_{55}) - \rho\tilde{v}^2
\end{vmatrix} = 0. \tag{23}
$$

To solve the complex eigenvalue problem and to find the roots, Wolfram Mathematica 10 was used.

As result, one obtains as roots

$$
\Lambda_{1,2} = \frac{1}{4}\left(\tilde{C}_{11} + \tilde{C}_{33} + 2\tilde{C}_{55} \pm \sqrt{\tilde{C}_{11}^2 + 4\tilde{C}_{13}^2 - 2\tilde{C}_{11}\tilde{C}_{33} + \tilde{C}_{33}^2 + 8\tilde{C}_{13}\tilde{C}_{55} + 4\tilde{C}_{55}^2} - 4\rho\tilde{v}^2\right), \tag{24}
$$

$$
\Lambda_3 = \frac{\tilde{C}_{44} + \tilde{C}_{66}}{2} - \rho\tilde{v}^2,
$$

with the corresponding eigenvectors

$$
\xi_{1,2} = \left(-\frac{-\tilde{C}_{11} + \tilde{C}_{33} \mp \sqrt{\tilde{C}_{11}^2 + 4\tilde{C}_{13}^2 - 2\tilde{C}_{11}\tilde{C}_{33} + \tilde{C}_{33}^2 + 8\tilde{C}_{13}\tilde{C}_{55} + 4\tilde{C}_{55}^2}}{2(\tilde{C}_{13} + \tilde{C}_{55})}, 0, 1\right)^T,
$$

$$
\xi_3 = (0, 1, 0)^T.
$$

Thereby, Λ_3 is assigned to the SH mode, because the corresponding eigenvector ξ_3 provides the particle displacements occurring perpendicular to the propagation direction polarized in x_2-direction. The eigenvalue of Λ_1 of the form $\Lambda_1 = \cdots + \sqrt{}$ relates to the quasilongitudinal mode, while the second eigenvalue of the form $\Lambda_2 = \cdots - \sqrt{}$ relates to the quasi-shear mode, because the longitudinal wave velocity has to be larger than the shear one, so that $v_L > v_T$. The results were verified following [16], p.390-391.

Finding the root of Equation (24), one obtains

$$
\tilde{C}_{13} = -\tilde{C}_{55} + \sqrt{\tilde{C}_{11}\tilde{C}_{33} + \tilde{C}_{11}\tilde{C}_{55} + \tilde{C}_{33}\tilde{C}_{55} + \tilde{C}_{55}^2 - 2\tilde{C}_{11}\rho\tilde{v}_L^2(45°) - 2\tilde{C}_{33}\rho\tilde{v}_L^2(45°) - 4\tilde{C}_{55}\rho\tilde{v}_L^2(45°) + 4\rho^2\tilde{v}_L^4(45°)}
$$

or

$$
\tilde{C}_{13} = -\tilde{C}_{55} + \sqrt{\tilde{C}_{11}\tilde{C}_{33} + \tilde{C}_{11}\tilde{C}_{55} + \tilde{C}_{33}\tilde{C}_{55} + \tilde{C}_{55}^2 - 2\tilde{C}_{11}\rho\tilde{v}_{SV}^2(45°) - 2\tilde{C}_{33}\rho\tilde{v}_{SV}^2(45°) - 4\tilde{C}_{55}\rho\tilde{v}_{SV}^2(45°) + 4\rho^2\tilde{v}_{SV}^4(45°)}.
$$

In the implemented calculation, the shear case was used, because a more precise result is expected. Real and imaginary part of $\tilde{C}_{13}$ could be separated after calculation.

For the determination of C_{12}, the symmetry condition $C_{12} = C_{11} - 2C_{66}$ is used. This condition is also valid for the imaginary part, so that $C_{12}^I = C_{11}^I - 2C_{66}^I$.

Looking at the horizontal alignment of columnar crystals, the symmetry condition $\bar{C}_{23} = \bar{C}_{22} - 2\bar{C}_{44}$ has to be used.

All together, the complex stiffness matrix results in

$$
\begin{bmatrix}
\rho\mathrm{Re}[\tilde{v}_L^2(90°)] & C_{11}-2C_{66} & C_{13} & & & \\
C_{11}-2C_{66} & \rho\mathrm{Re}[\tilde{v}_L^2(90°)] & C_{13} & & & \\
C_{13} & C_{13} & \rho\mathrm{Re}[\tilde{v}_L^2(0°)] & & & \\
& & & \rho\mathrm{Re}[\tilde{v}_{SH}^2(0°)] & & \\
& & & & \rho\mathrm{Re}[\tilde{v}_{SV}^2(90°)] & \\
& & & & & \rho\mathrm{Re}[\tilde{v}_{SH}^2(90°)]
\end{bmatrix}
$$

$$
+\, i
\begin{bmatrix}
\rho\mathrm{Im}[\tilde{v}_L^2(90°)] & C_{11}^I-2C_{66}^I & C_{13}^I & & & \\
C_{11}^I-2C_{66}^I & \rho\mathrm{Im}[\tilde{v}_L^2(90°)] & C_{13}^I & & & \\
C_{13}^I & C_{13}^I & \rho\mathrm{Im}[\tilde{v}_L^2(0°)] & & & \\
& & & \rho\mathrm{Im}[\tilde{v}_{SH}^2(0°)] & & \\
& & & & \rho\mathrm{Im}[\tilde{v}_{SV}^2(90°)] & \\
& & & & & \rho\mathrm{Im}[\tilde{v}_{SH}^2(90°)]
\end{bmatrix},
\tag{25}
$$

in case of a vertical alignment of the columnar crystals.

For a calculation of the complex stiffness matrix in the case of a horizontal arrangement of the columnar crystals, all angles could be rotated by 90°, as described in chapter 3.1.2, but the symmetry conditions have to be considered.

The ultrasonic velocities, wavenumbers and attenuations for the different directions and modes are given from scattering theory in section 3.1, thus the complex stiffness matrix can be calculated.

6 Implemented programs

All calculations were implemented in MATLAB R2019a. For the calculation of complex wavenumbers two program versions were implemented. One version with a graphical interface for easy input of parameters and user-friendly control of the calculation is well suited for internal use in the GPSS algorithm, because all values of the complex wave number can be exported as txt-file. In addition, it is also suitable for external use to compare theory and measurement, because this version was extended by a graph, which contains the conversion in dB/m (cf. chapter 3.3). The second version is a batch version that is suitable for a plug-in into CIVA. Additionally, a batch version has been implemented as a plug-in to CIVA for the calculation of the complex stiffness matrix.

All versions were packed as separate executables. To run the executables the version 9.6 (R2019a) of the MATLAB Runtime has to be installed. The MATLAB Runtime installer can be downloaded for free under http://www.mathworks.com/products/compiler/mcr/index.html.

6.1 Version with Graphical User Interface (GUI)

Files to Package for Standalone application

– CalcComplexK_GUI.exe
– readme.txt
– Materialliste.txt
– splash.png

Execution and Functionality

To execute the standalone application correctly, a Materialliste.txt file is required in the same folder. Then the executable can be run. When executed, a splash display is briefly shown to indicate the loading process. A short time later, a graphical user interface (GUI) is opened (cf. Figure 13). With the GUI, the input and calculation can be controlled. One has to choose a material from a list or to edit the input fields for selection of materials. As a second step, the orientation of the columnar crystals has to be selected. Then the calculation can be started with the button 'calculate'. If a field of input parameters in selection of materials or in measurement parameters has been edited, one has to push the button again to activate the modification. If the button 'save' is used, result files are saved as *.txt. Two separate files, one file with real part and one file with imaginary part of the calculated solution is stored. The solution is a column vector divided into the individual angular steps that were entered. In addition, one file each with the real and imaginary part of the isotropic angle-independent solution is saved. All values are stored in the unit $\frac{1}{mm}$.
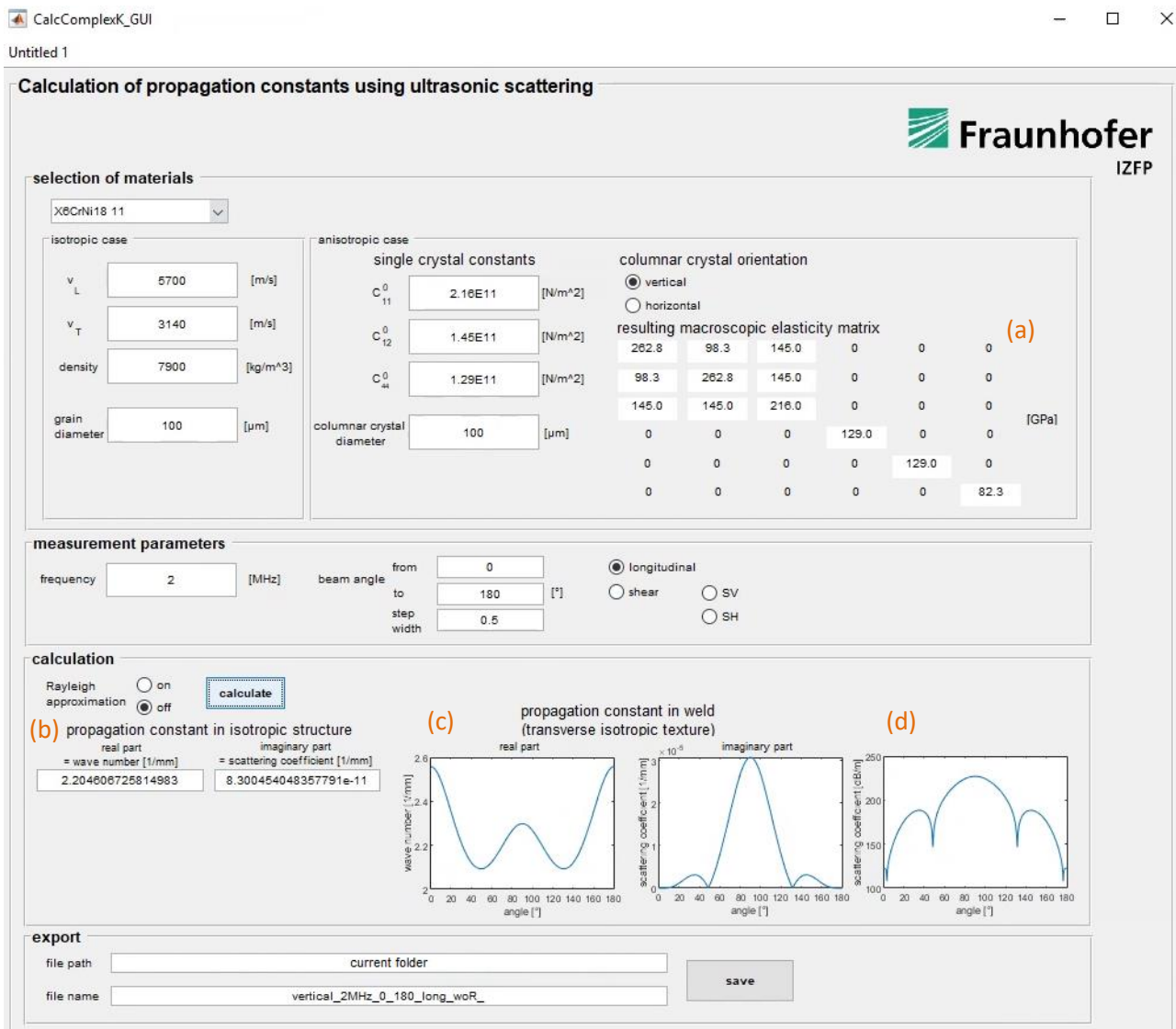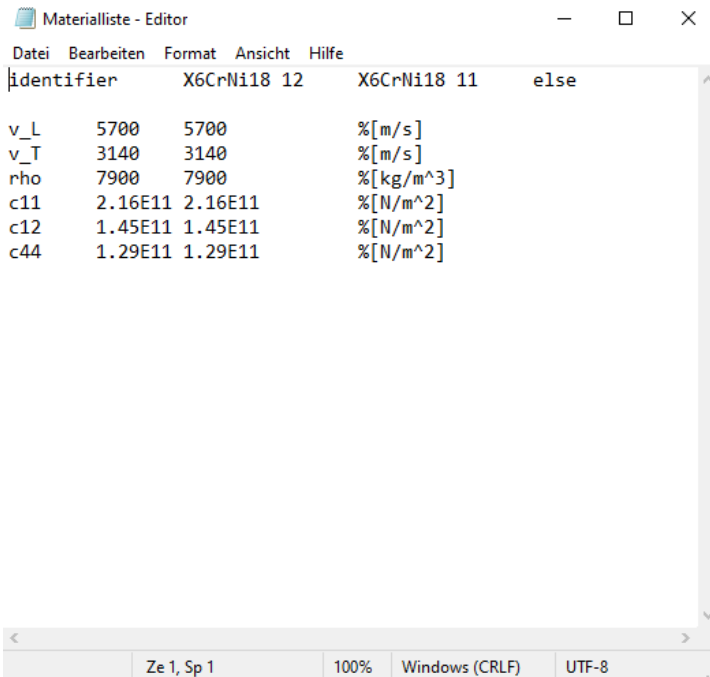
Figure 13 : graphical user interface for user-friendly handling of the calculation of complex wavenumbers

Part (a) of Figure 13 shows the calculation of the stiffness matrix according to Bunge (see chapter 4). Part (c) gives the calculation of the complex wavenumber in textured media (see chapter 3.1), while part (b) gives the complex wavenumber in isotropic case determined after [4, 5]. For textured media the complex wavenumber is plotted separately for the real part and the imaginary part depending on the angle. The real part gives the wavenumber and the imaginary part the scattering coefficient α_s, which describes the attenuation due to ultrasonic scattering. This value was converted to dB/m in part (d), as described in chapter 3.3, to allow easier comparison with measured values.

List of materials

To have the opportunity to select different materials from a list, it is necessary to use a Materialliste.txt file of the form shown in Figure 14. It gives a list of materials and its data. The list can be extended as long as the structure is maintained.

Figure 14 : Materialliste.txt

6.2   Batch version for complex wavenumber

The batch version has the same functionality as the GUI version, but instead of the Materialliste.txt a txt-file for all input parameters is used.

Files to Package for Standalone

- CalcComplexK_App.exe
- readme.txt
- Input.txt
- splash.png

Execution and Functionality

To execute the standalone application correctly, an Input.txt with the structure as described in the following section is necessary. The input file is required to be in the same folder. Then the executable can be run. When executed, a splash display is briefly shown to indicate the calculation process. A short time later, the result files are saved as *.txt in the folder of the app. Two separate files, one file with real part and one file with imaginary part of the calculated solution is stored. The solution is a column vector, divided into the individual angular steps that were entered. All values are saved with the unit $\frac{1}{mm}$. In addition, a file is produced which contains the used elasticity matrix (calculated after Bunge, cf. chapter 4) in $\frac{N}{m^2}$.

Input File

The input file must contain the following parameters:

- isotropic longitudinal wave velocity: c_L in $\frac{m}{s}$
- isotropic shear wave velocity: c_T in $\frac{m}{s}$
- density of the material: ρ in $\frac{kg}{m^3}$
- the single crystal constants for cubic crystals: C_{11}^0, C_{12}^0, C_{44}^0 in $\frac{N}{m^2}$
- grain diameter in isotropic case: ssd in micrometer
- columnar crystal diameter for calculation of anisotropic case: ccd in micrometer
- measurement frequency: f in MHz
- angles of incident wave in relation to the columnar crystal axis:

from ia_lb in degree

to ia_ub in degree

with a stepwith ia_step in degree

– one can choose the orientation of columnar crystals between:

vertical:	orientation = 1
horizontal:	orientation = 2

– one can choose the mode of transmitted wave:
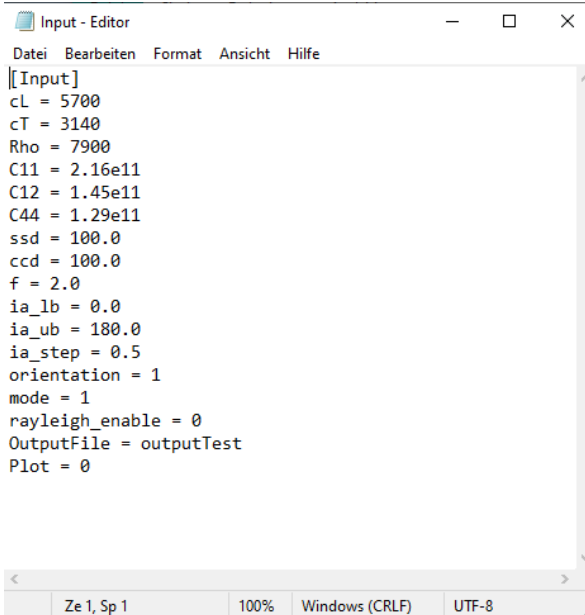
longitudinal:		mode = 1
shear:	SV	mode = 2
	SH	mode = 3

– one can choose, if Rayleigh approximation should be used:

Rayleigh off:	rayleigh_enable = 0
Rayleigh on:	rayleigh_enable = 1

– one can choose a name for output file, which will be stored in the same folder as the application file:

OutputFile

– for testing one can choose whether a plot should be opened in addition to the output file:

no plot:	Plot = 0
plot:	Plot = 1

An example is given in Figure 15.

Figure 15 : example of an input file

6.3 Batch version for complex stiffness matrix

The batch version for a calculation of the complex stiffness matrix is realized in the same manner as the batch version for the complex wavenumber, but in addition with the calculation described in chapter 5.

Files to Package for Standalone

– CalcComplexStiffness.exe
– readme.txt
– Input.txt
– splash.png

Execution and Functionality

To execute the standalone application correctly, an Input.txt with the structure as described in the following section is necessary. The Input file is required in the same folder. Then the executable can be run. When

executed, a splash display is briefly shown to indicate the calculation process. A short time later, the result file is saved as *.txt in the folder of the app. One file containing the complex stiffness matrix will be stored. The solution is a space-separated matrix, divided into the real and imaginary part. The imaginary part is indicated by a +i in front of it. The complex stiffness matrix is stored in $\frac{N}{m^2}$.

Input File

The input file must contain the following parameters:

- isotropic longitudinal wave velocity: c_L in $\frac{m}{s}$
- isotropic shear wave velocity: c_T in $\frac{m}{s}$
- density of the material: ρ in $\frac{kg}{m^3}$
- the single crystal constants for cubic crystals: C_{11}^0, C_{12}^0, C_{44}^0 in $\frac{N}{m^2}$
- grain diameter in isotropic case: ssd in micrometer
- columnar crystal diameter for calculation of anisotropic case: ccd in micrometer
- measurement frequency: f in MHz
- one can choose the orientation of columnar crystals between:

vertical:	orientation = 1
horizontal:	orientation = 2

- one can choose, if Rayleigh approximation should be used:

Rayleigh off:	rayleigh_enable = 0
Rayleigh on:	rayleigh_enable = 1

- one can choose a name for output file, which will be stored in the same folder as the application file:

OutputFile

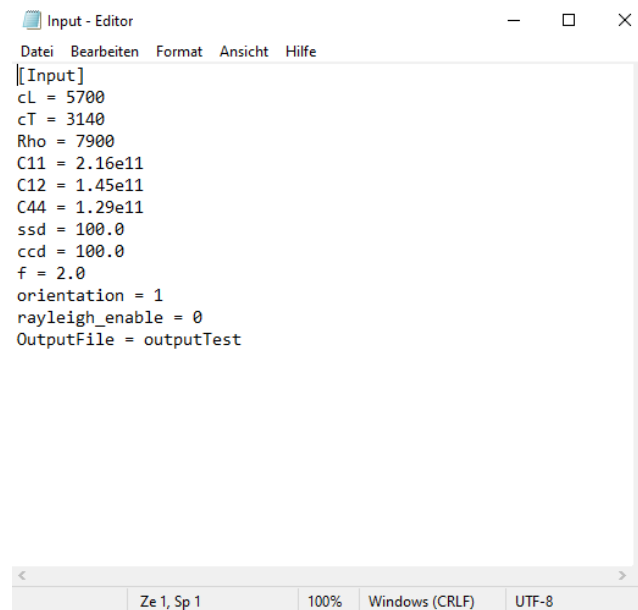An example is given in Figure 16.

Figure 16 : example of an input file

Example of results

An example of a calculated complex stiffness matrix is given in Figure 17. The same data were used as in the example in section 3.3 for a vertical weld made of X6CrNi18 11 with the material data from Table 1 and a frequency of 2MHz. A Rayleigh approximation was not used.

```
2.36342649E+11  9.49776763E+10  1.53525938E+11  0.00000000E+00  0.00000000E+00  0.00000000E+00
9.49776763E+10  2.36342649E+11  1.53525938E+11  0.00000000E+00  0.00000000E+00  0.00000000E+00
1.53525938E+11  1.53525938E+11  1.91175165E+11  0.00000000E+00  0.00000000E+00  0.00000000E+00
0.00000000E+00  0.00000000E+00  0.00000000E+00  1.09560848E+11  0.00000000E+00  0.00000000E+00
0.00000000E+00  0.00000000E+00  0.00000000E+00  0.00000000E+00  1.09560961E+11  0.00000000E+00
0.00000000E+00  0.00000000E+00  0.00000000E+00  0.00000000E+00  0.00000000E+00  7.06824865E+10
+i
6.26685570E+06  -1.33483319E+08  -4.21169835E+07  0.00000000E+00  0.00000000E+00  0.00000000E+00
-1.33483319E+08  6.26685570E+06  -4.21169835E+07  0.00000000E+00  0.00000000E+00  0.00000000E+00
-4.21169835E+07  -4.21169835E+07  3.35558040E+02  0.00000000E+00  0.00000000E+00  0.00000000E+00
0.00000000E+00  0.00000000E+00  0.00000000E+00  2.75609977E+02  0.00000000E+00  0.00000000E+00
0.00000000E+00  0.00000000E+00  0.00000000E+00  0.00000000E+00  6.38388911E+01  0.00000000E+00
0.00000000E+00  0.00000000E+00  0.00000000E+00  0.00000000E+00  0.00000000E+00  6.98750871E+07
```

Figure 17 : calculated stiffness matrix for vertical oriented austenitic weld X6 CrNi 18 11

It can already be seen from chapter 3.3 that especially the attenuation values for the quasi-longitudinal wave in 0°-direction, for the SH wave in 0°-direction and the quasi-shear wave in 0° and 90°-direction are underestimated. This leads to significantly lower values for the entries C_{33}^I, C_{44}^I and C_{55}^I (see (25), chapter 5). Nevertheless, all values of the imaginary part lie in similar ranges as in [12] and [17], although these are difficult to compare due to the different materials.

7 Conclusion

All necessary values could be derived from the analytical scattering theory. Two cases were considered for the textured structure, the vertical and the horizontal case. For comparison with measured values a scaling in dB/m was determined, which was verified using measured values from the literature. This comparison showed a good agreement between theory and measurement, although this could be further improved by taking into account the angle of aperture of the sound beam done in a postprocessing process. The largest deviation between theoretical and measured values is recognized for the quasi-longitudinal wave in 0°-direction, parallel to the columnar crystals. Also the shear horizontal wave in 0°-direction and the vertical polarized quasi-shear wave in 0° and 90°-direction show deviations. This leads to underestimated values in three entries of the complex stiffness matrix, calculated by the complex wavenumbers from scattering theory. Nevertheless, the calculated stiffness matrix can be used for a plug-in in CIVA, since all values are within the plausible value range. These numerical validations will be done next.

8 Bibliography

[1] S. Hirsekorn, "Directional dependence of ultrasonic propagation in textured polycrystals," *The Journal of the Acoustical Society of America*, vol. 79, no. 5, pp. 1269–1279, 1986, doi: 10.1121/1.393706.

[2] S. Hirsekorn, "Theoretical Description of Ultrasonic Propagation and Scattering Phenomena in Polycrystalline Structures Aiming for Simulations on Nondestructive Materials Characterization: European Conference on Nondestructive Testing (11), 06.-10.10.2014, Prag," in *European Conference on Nondestructive Testing (11)*, Brno, 2014, contribution 331.

[3] S. Hirsekorn, "The scattering of ultrasonic waves in polycrystalline materials with texture," *The Journal of the Acoustical Society of America*, vol. 77, no. 3, pp. 832–843, 1985, doi: 10.1121/1.392052.

[4] S. Hirsekorn, "The scattering of ultrasonic waves by polycrystals," *The Journal of the Acoustical Society of America*, vol. 72, no. 3, pp. 1021–1031, 1982, doi: 10.1121/1.388233.

[5] S. Hirsekorn, "The scattering of ultrasonic waves by polycrystals. II. Shear waves," *The Journal of the Acoustical Society of America*, vol. 73, no. 4, pp. 1160–1163, 1983, doi: 10.1121/1.389206.

[6] S. Hirsekorn, "Ausbreitung ebener Schallwellen im austenitischen Schweissgut, einem anisotropen, polykristallinen Material mit zylindersymmetrischer Textur," in *Ultraschallprüfung von austenitischen Plattierungen, Mischnähten und austenitischen Schweissnähten*, 1995, S. 159-195.

[7] J. Krautkrämer and H. Krautkrämer, *Ultrasonic testing of materials,* 4th ed. Berlin: Springer, 1990.

[8] H.-J. Bunge, *Texture analysis in materials science*. London: Butterworths, 1982.

[9] J. Li, L. Yang, and S. I. Rokhlin, "Effect of texture and grain shape on ultrasonic backscattering in polycrystals," *Ultrasonics*, vol. 54, no. 7, pp. 1789–1803, 2014, doi: 10.1016/j.ultras.2014.02.020.

[10] J. Li and S. I. Rokhlin, "Elastic wave scattering in random anisotropic solids," *International Journal of Solids and Structures*, 78-79, pp. 110–124, 2016, doi: 10.1016/j.ijsolstr.2015.09.011.

[11] Jens Prager, "Bildgebende Ultraschallprüfung von austenitischen Schweißnähten," 20. Workshop „Physikalische Akustik", Schallausbreitung in inhomogenen Medien. Physikzentrum Bad Honnef, Nov. 14 2013.

[12] B. Chassignole, V. Duwig, M.-A. Ploix, P. Guy, and R. El Guerjouma, "Modelling the attenuation in the ATHENA finite elements code for the ultrasonic testing of austenitic stainless steel welds," *Ultrasonics*, vol. 49, no. 8, pp. 653–658, 2009, doi: 10.1016/j.ultras.2009.04.001.

[13] S. Baudouin and B. Hosten, "Immersion ultrasonic method to measure elastic constants and anisotropic attenuation in polymer-matrix and fiber-reinforced composite materials," *Ultrasonics*, vol. 34, 2-5, pp. 379–382, 1996, doi: 10.1016/0041-624X(96)00021-2.

[14] B. Hosten, "Reflection and transmission of acoustic plane waves on an immersed orthotropic and viscoelastic solid layer," *The Journal of the Acoustical Society of America*, vol. 89, no. 6, pp. 2745–2752, 1991, doi: 10.1121/1.400685.

[15] Y. Zhu and I. Tsvankin, "Plane-wave propagation in attenuative transversely isotropic media," *GEOPHYSICS*, vol. 71, no. 2, T17-T30, 2006, doi: 10.1190/1.2187792.

[16] B. Auld, *Acoustic fields and waves in solids. Vol. I (2nd Edition),* 2nd ed. Malabar: Krieger Publishing Company, 1990.

[17] R. Shane Fazzio, "A derivation of the Christoffel equation with damping," *Ultrasonics*, vol. 45, 1-4, pp. 196–207, 2006, doi: 10.1016/j.ultras.2006.09.005.

9 Annex

9.1 Calculation of $< C_{ijkl} >$

In the following, $< C_{ijkl} >$ were calculated after (13) with the mean values of a multiple products of rotation matrix elements $a_{\alpha i}$ after [1, 3].

The mean value of a multiple product of rotation matrix elements $a_{\alpha i}$ results in:

$$\sum_{\alpha=1}^{3} < a_{\alpha 1}^4 > = \frac{3}{5} + \frac{1}{10\sqrt{3 \cdot 7}} C_4^{10} - \frac{1}{3\sqrt{3 \cdot 5 \cdot 7}} C_4^{11} + \frac{1}{6\sqrt{3 \cdot 5}} C_4^{12}$$

$$\sum_{\alpha=1}^{3} < a_{\alpha 2}^4 > = \frac{3}{5} + \frac{1}{10\sqrt{3 \cdot 7}} C_4^{10} + \frac{1}{3\sqrt{3 \cdot 5 \cdot 7}} C_4^{11} + \frac{1}{6\sqrt{3 \cdot 5}} C_4^{12}$$

$$\sum_{\alpha=1}^{3} < a_{\alpha 3}^4 > = \frac{3}{5} + \frac{4}{15\sqrt{3 \cdot 7}} C_4^{10}$$

$$\sum_{\alpha=1}^{3} < a_{\alpha 1}^2 a_{\alpha 2}^2 > = \frac{1}{5} + \frac{1}{30\sqrt{3 \cdot 7}} C_4^{10} - \frac{1}{6\sqrt{3 \cdot 5}} C_4^{12} \tag{26}$$

$$\sum_{\alpha=1}^{3} < a_{\alpha 1}^2 a_{\alpha 3}^2 > = \frac{1}{5} - \frac{2}{15\sqrt{3 \cdot 7}} C_4^{10} + \frac{1}{3\sqrt{3 \cdot 5 \cdot 7}} C_4^{11}$$

$$\sum_{\alpha=1}^{3} < a_{\alpha 2}^2 a_{\alpha 3}^2 > = \frac{1}{5} - \frac{2}{15\sqrt{3 \cdot 7}} C_4^{10} - \frac{1}{3\sqrt{3 \cdot 5 \cdot 7}} C_4^{11}$$

$$\sum_{\alpha=1}^{3} < a_{\alpha i} a_{\alpha j} a_{\alpha k} a_{\alpha l} > = 0 \quad \text{else.}$$

9.1.1 Calculation of $< C_{ijkl} >$ for vertical transversely isotropic texture

Using (26) with $C_4^{11} = 0$ and $C_4^{12} = 0$ due to transversely isotropic structure in x_3-direction, $< C_{ijkl} >$ could be calculated after (13):

$$< C_{1111} > = < C_{2222} > = C_{12}^0 + 2C_{44}^0 + (C_{11}^0 - C_{12}^0 - 2C_{44}^0) \sum_{\alpha=1}^{3} < a_{\alpha 1}^4 > \tag{27}$$

$$= C_{11}^0 + A \left(-\frac{2}{5} + \frac{1}{10\sqrt{3\cdot 7}} C_4^{10} \right)$$

$$< C_{3333} > = C_{12}^0 + 2C_{44}^0 + A \sum_{\alpha=1}^{3} < a_{\alpha 3}^4 > \tag{28}$$

$$= C_{11}^0 + A \left(-\frac{2}{5} + \frac{4}{15\sqrt{3\cdot 7}} C_4^{10} \right)$$

$$< C_{1122} > = C_{12}^0 + A \sum_{\alpha=1}^{3} < a_{\alpha 1}^2 a_{\alpha 2}^2 > \tag{29}$$

$$= C_{12}^0 + A \left(\frac{1}{5} + \frac{1}{30\sqrt{3\cdot 7}} C_4^{10} \right)$$

$$< C_{1133} > = < C_{2233} > = C_{12}^0 + A \sum_{\alpha=1}^{3} < a_{\alpha 1}^2 a_{\alpha 3}^2 > \tag{30}$$

$$= C_{12}^0 + A \left(\frac{1}{5} - \frac{2}{15\sqrt{3\cdot 7}} C_4^{10} \right)$$

$$< C_{2323} > = < C_{1313} > = C_{44}^0 + A \sum_{\alpha=1}^{3} < a_{\alpha 2}^2 a_{\alpha 3}^2 > \tag{31}$$

$$= C_{44}^0 + A \left(\frac{1}{5} - \frac{2}{15\sqrt{3\cdot 7}} C_4^{10} \right)$$

$$< C_{1212} > = C_{44}^0 + A \sum_{\alpha=1}^{3} < a_{\alpha 1}^2 a_{\alpha 2}^2 > \tag{32}$$

$$= C_{44}^0 + A \left(\frac{1}{5} + \frac{1}{30\sqrt{3\cdot 7}} C_4^{10} \right),$$

so that $< C_{1212} > = \frac{1}{2}(< C_{1111} > - < C_{1122} >)$ is satisfied.

9.1.2 Calculation of $< C_{ijkl} >$ for horizontal transversely isotropic texture

Since the equations in (14) are valid for the orthotropic case, they can also be used in the horizontal transversely isotropic case with equations (27)-(32) to calculate the $< C_{ijkl} >$. However, other texture parameters C_4^{10}, C_4^{11} and C_4^{12} are valid. These are derived in the following from the relationship between horizontal and vertical texture. For the elastic constants, the relationship has to be:

$$\bar{C}_{11} = C_{33} \tag{33}$$

$$\bar{C}_{22} = \bar{C}_{33} = C_{11} \tag{34}$$

$$\bar{C}_{44} = C_{66} \tag{35}$$

$$\bar{C}_{55} = \bar{C}_{66} = C_{44} = C_{55} \tag{36}$$

Using the general texture dependent formulation for $< C_{ijkl} >$:

$$< C_{1111} > = C_{12}^0 + 2C_{44}^0 + A \left(\frac{3}{5} + \frac{1}{10\sqrt{3\cdot 7}} C_4^{10} - \frac{1}{3\sqrt{3\cdot 5\cdot 7}} C_4^{11} + \frac{1}{6\sqrt{3\cdot 5}} C_4^{12} \right) \tag{37}$$

$$< C_{2222} > = C_{12}^0 + 2C_{44}^0 + A \left(\frac{3}{5} + \frac{1}{10\sqrt{3\cdot 7}} C_4^{10} + \frac{1}{3\sqrt{3\cdot 5\cdot 7}} C_4^{11} + \frac{1}{6\sqrt{3\cdot 5}} C_4^{12} \right) \tag{38}$$

$$< C_{3333} > = C_{12}^0 + 2C_{44}^0 + A \left(\frac{3}{5} + \frac{4}{15\sqrt{3 \cdot 7}} C_4^{10} \right) \tag{39}$$

In accordance with (34) results from $\bar{C}_{22} = C_{11} = C_{11}^0 - \frac{1}{4}A = C_{12}^0 + 2C_{44}^0 + \frac{3}{4}A$ with (39), C_4^0 in:

$$C_4^{10} = \frac{9}{16}\sqrt{3 \cdot 7}.$$

From (33) implies that $\bar{C}_{11} = C_{33} = C_{11}^0$ is only valid, if $\frac{3}{5} + \frac{1}{10\sqrt{3 \cdot 7}} C_4^{10} - \frac{1}{3\sqrt{3 \cdot 5 \cdot 7}} C_4^{11} + \frac{1}{6\sqrt{3 \cdot 5}} C_4^{12} = 1$

and $\bar{C}_{22} = C_{11} = C_{11}^0 - \frac{1}{4}A$ is only valid, if $\frac{3}{5} + \frac{1}{10\sqrt{3 \cdot 7}} C_4^{10} + \frac{1}{3\sqrt{3 \cdot 5 \cdot 7}} C_4^{11} + \frac{1}{6\sqrt{3 \cdot 5}} C_4^{12} = \frac{3}{4}$. In combination we obtain:

$$C_4^{11} = -\frac{3}{8}\sqrt{3 \cdot 5 \cdot 7}$$

With C_4^{10}, C_4^{11} and the condition $< C_{2222} > = < C_{3333} >$ regarding $\bar{C}_{22} = \bar{C}_{33}$, C_4^{12} results in:

$$C_4^{12} = \frac{21}{16}\sqrt{3 \cdot 5}.$$

Hence, the conditions (35) and (36) will be fulfilled.

9.2   The infinite series of spherical Bessel and Hankel functions

Define $j_l(x)$ and $h_l^{(2)}(x)$ as spherical Bessel and Hankel functions of the second kind, then the infinite series $\bar{M}$ and $\widetilde{M}$ are given by

$$
\begin{aligned}
\bar{M}_{MMMM} = \sum_l \Bigg\{ & 4\, \frac{l(l-1)(l+1)(l+2)}{(k_M a)^4} j_{l+1}(k_M a) j_{l-1}(k_M a) \\
& + (2l+1)\left[2\big(j_l(k_M a)\big)^2 - j_{l+1}(k_M a) j_{l-1}(k_M a)\right] \\
& - i(k_M a)^3 \Bigg\{ \frac{2l+1}{2}\left[\big(j_l(k_M a)\big)^2 - j_{l+1}(k_M a) j_{l-1}(k_M a)\right]\left[2 h_l^{(2)}(k_M a) j_l(k_M a)\right. \\
& - h_{l+1}^{(2)}(k_M a) j_{l-1}(k_M a) - h_{l-1}^{(2)}(k_M a) j_{l+1}(k_M a)\Big] \\
& - \frac{l(l-1)(l+1)(l+2)}{2l+1} \frac{4}{(k_M a)^4}\left[h_{l+1}^{(2)}(k_M a) j_{l-1}(k_M a)\right. \\
& + h_{l-1}^{(2)}(k_M a) j_{l+1}(k_M a)\Big] j_{l-1}(k_M a) j_{l+1}(k_M a) \\
& - 24 \frac{l(l+1)(2l+1)}{(2l-1)(2l+3)} \frac{l^2+l-1}{(k_M a)^4} \big(j_l(k_M a)\big)^3 h_l^{(2)}(k_M a) \Bigg\} \Bigg\},
\end{aligned}
$$

with

$$\bar{M}_{iiii} = \bar{M}_{iijj} + 2\,\bar{M}_{ijij} = 3\,\bar{M}_{ijij}$$

and

$$
\begin{aligned}
\bar{M}_{MMii} = \sum_l \Bigg\{ & -2\, \frac{l(l-1)(l+1)(l+2)}{(k_M a)^4} j_{l+1}(k_M a) j_{l-1}(k_M a) \\
& - i\, \frac{2l(l+1)}{k_M a}\left[\frac{(l-1)(l+2)}{2l+1}\left(h_{l+1}^{(2)}(k_M a) j_{l-1}(k_M a)\right.\right. \\
& + h_{l-1}^{(2)}(k_M a) j_{l+1}(k_M a)\Big) j_{l-1}(k_M a) j_{l+1}(k_M a) \\
& + \frac{(2l+1)(2l^2+2l-3)}{(2l-1)(2l+3)} \big(j_l(k_M a)\big)^3 h_l^{(2)}(k_M a) \Bigg] \Bigg\},
\end{aligned}
$$

with

$$\bar{M}_{iiMM} = \bar{M}_{MMii}, \quad \bar{M}_{iMiM} = \bar{M}_{MMii}$$

and

$$\bar{M}_{ijij} = \sum_l \left\{ \frac{1}{2} \frac{l(l-1)(l+1)(l+2)}{(k_M a)^4} j_{l+1}(k_M a) j_{l-1}(k_M a) \right.$$

$$+ i \frac{l(l+1)}{k_M a} \left[\frac{(l-1)(l+2)}{2(2l+1)} \left(h_{l+1}^{(2)}(k_M a) j_{l-1}(k_M a) \right. \right.$$

$$+ h_{l-1}^{(2)}(k_M a) j_{l+1}(k_M a) \Big) j_{l-1}(k_M a) j_{l+1}(k_M a)$$

$$\left. \left. - \frac{l(l+1)(2l+1)}{(2l-1)(2l+3)} \left(j_l(k_M a) \right)^3 h_l^{(2)}(k_M a) \right] \right\},$$

with

$$\bar{M}_{iijj} = \bar{M}_{ijij}.$$

The terms $\widetilde{M}$ contains additionally to the longitudinal wavenumbers k_M the shear wavenumbers κ_I:

$$\widetilde{M}_{MMMM} = \sum_l \left\{ \frac{k_M^2}{\kappa_I^2} \frac{l(l-1)(l+1)(l+2)}{(k_M a)^4} j_{l+1}(k_M a) j_{l-1}(k_M a) \right.$$

$$+ \frac{k_M^2}{k_M^2 - \kappa_I^2} \frac{(2l+1)}{2} \left[\left(j_l(k_M a) \right)^2 - j_{l+1}(k_M a) j_{l-1}(k_M a) \right]$$

$$- i\kappa_I a \left\{ (2l+1) \frac{\kappa_I^2}{(k_M^2 - \kappa_I^2)^2} \left[\frac{k_M}{\kappa_I} j_l(\kappa_I a) j_{l+1}(k_M a) \right. \right.$$

$$- j_{l+1}(\kappa_I a) j_l(k_M a) \Big] \left[\frac{k_M}{\kappa_I} h_l^{(2)}(\kappa_I a) j_{l+1}(k_M a) - h_{l+1}^{(2)}(\kappa_I a) j_l(k_M a) \right]$$

$$- \frac{l(l-1)(l+1)(l+2)}{2l+1} \frac{1}{(k_M a)^2} \left[h_{l+1}^{(2)}(\kappa_I a) j_{l-1}(\kappa_I a) \right.$$

$$+ h_{l-1}^{(2)}(\kappa_I a) j_{l+1}(\kappa_I a) \Big] j_{l-1}(k_M a) j_{l+1}(k_M a)$$

$$\left. \left. - 6 \frac{l(l+1)(2l+1)}{(2l-1)(2l+3)} \frac{l^2+l-1}{(k_M a)^2} j_l(\kappa_I a) h_l^{(2)}(\kappa_I a) \left(j_l(k_M a) \right)^2 \right\} \right\},$$

with

$$\widetilde{M}_{iiii} = \widetilde{M}_{iijj} + 2\,\widetilde{M}_{ijij} = 3\,\widetilde{M}{ijij}$$

and

$$\widetilde{M}_{MMii} = \sum_l \left\{ -\frac{1}{2} \frac{k_M^2}{\kappa_I^2} \frac{l(l-1)(l+1)(l+2)}{(k_M a)^4} j_{l+1}(k_M a) j_{l-1}(k_M a) \right.$$

$$- i \frac{l(l+1)}{2k_M a} \frac{\kappa_I}{k_M} \left[\frac{(l-1)(l+2)}{2l+1} \left(h_{l+1}^{(2)}(\kappa_I a) j_{l-1}(\kappa_I a) \right. \right.$$

$$- h_{l-1}^{(2)}(\kappa_I a) j_{l+1}(\kappa_I a) \Big) j_{l-1}(k_M a) j_{l+1}(k_M a)$$

$$\left. \left. + \frac{(2l+1)(2l^2+2l-3)}{(2l-1)(2l+3)} j_l(\kappa_I a) h_l^{(2)}(\kappa_I a) \left(j_l(k_M a) \right)^2 \right] \right\},$$

with

$$\widetilde{M}_{iiMM} = \widetilde{M}_{MMii}, \quad \widetilde{M}_{iMiM} = \widetilde{M}_{MMii}$$

and

$$\widetilde{M}_{ijij} = \sum_l \left\{ \frac{1}{8} \frac{k_M^2}{\kappa_I^2} \frac{l(l-1)(l+1)(l+2)}{(k_M a)^4} j_{l+1}(k_M a) j_{l-1}(k_M a) \right.$$

$$+ i \frac{l(l+1)}{4 k_M a} \frac{\kappa_I}{k_M} \left[\frac{(l-1)(l+2)}{2(2l+1)} \left(h_{l+1}^{(2)}(\kappa_I a) j_{l-1}(\kappa_I a) \right. \right.$$

$$\left. - h_{l-1}^{(2)}(\kappa_I a) j_{l+1}(\kappa_I a) \right) j_{l-1}(k_M a) j_{l+1}(k_M a)$$

$$\left. \left. - \frac{l(l+1)(2l+1)}{(2l-1)(2l+3)} j_l(\kappa_I a) h_l^{(2)}(\kappa_I a) \left(j_l(k_M a) \right)^2 \right] \right\},$$

with

$$\widetilde{M}_{iijj} = \widetilde{M}_{ijij}.$$

These equations give the sums of the quantities $\bar{M}$ and $\widetilde{M}$ for longitudinal waves, which are required in section 3.1.1.1. To determine the sums for transverse waves required in section 3.1.1.2, the wavenumbers k_M must be replaced by κ_{MP} and κ_I by k_I in the constitutive equations.